

# Non-Coherent Over-the-Air Decentralized Gradient Descent

Nicolò Michelusi

**Abstract**—Decentralized Gradient Descent (DGD) is a popular algorithm used to solve decentralized optimization problems in diverse domains such as remote sensing, distributed inference, multi-agent coordination, and federated learning. Yet, executing DGD over wireless systems affected by noise, fading and limited bandwidth presents challenges, requiring scheduling of transmissions to mitigate interference and the acquisition of topology and channel state information – complex tasks in wireless decentralized systems. This paper proposes a DGD algorithm tailored to wireless systems. Unlike existing approaches, it operates without inter-agent coordination, topology information, or channel state information. Its core is a Non-Coherent Over-The-Air (NCOTA) consensus scheme, exploiting a *noisy energy superposition* property of wireless channels. With a randomized transmission strategy to accommodate half-duplex operation, transmitters map local optimization signals to energy levels across subcarriers in an OFDM frame, and transmit concurrently without coordination. It is shown that received energies form a noisy consensus signal, whose fluctuations are mitigated via a consensus stepsize. NCOTA-DGD leverages the channel pathloss for consensus formation, without explicit knowledge of the mixing weights. It is shown that, for the class of strongly-convex problems, the expected squared distance between the local and globally optimum models vanishes with rate  $\mathcal{O}(1/\sqrt{k})$  after  $k$  iterations, with a proper design of decreasing stepsizes. Extensions address a broad class of fading models and frequency-selective channels. Numerical results on an image classification task depict faster convergence vis-à-vis running time than state-of-the-art schemes, especially in densely deployed networks.

## I. INTRODUCTION

The proliferation of networks constituted of devices with sensing, computation and wireless communication capabilities, presents new opportunities in diverse domains such as remote sensing, distributed inference [3], multi-agent coordination [4], and machine learning (ML) [5]. In these domains,  $N$  devices cooperate to attain a common goal, by relying on local information and communications. Typically, this problem can be cast as that of finding a global  $\mathbf{w}^* \in \mathbb{R}^d$  solving

$$\mathbf{w}^* = \arg \min_{\mathbf{w} \in \mathbb{R}^d} F(\mathbf{w}), \text{ where } F(\mathbf{w}) \triangleq \frac{1}{N} \sum_{i=1}^N f_i(\mathbf{w}), \quad \{\mathbf{P}\}$$

$f_i(\mathbf{w})$  is a local function only known to node  $i$ ,  $\mathbf{w}$  is a  $d$ -dimensional model, so that  $F(\mathbf{w})$  is the network-wide objective. For instance, in ML applications,  $f_i(\mathbf{w}) = \frac{1}{|\mathcal{D}_i|} \sum_{\boldsymbol{\xi} \in \mathcal{D}_i} \phi(\boldsymbol{\xi}; \mathbf{w})$  is the empirical loss over the local dataset  $\mathcal{D}_i$ , with loss function  $\phi(\boldsymbol{\xi}; \mathbf{w})$  on the datapoint  $\boldsymbol{\xi}$ .

Yet, significant challenges emerge in solving  $\{\mathbf{P}\}$ , associated with the decentralized nature of the system and resource-limited wireless connectivity. Federated learning (FL) solves  $\{\mathbf{P}\}$  based on a client-server architecture, in which the  $N$  edge devices (the clients) interact over multiple rounds with a parameter server (PS, such as a base station), acting as a model aggregator. Nevertheless, the FL architecture encounters

several challenges in wireless scenarios: 1) devices far away from the PS (e.g., in rural environments), may suffer from severe pathloss conditions and blockages [6]; 2) uplink communications to the PS may be a severe bottleneck when  $N$  is large, due to bandwidth constraints [7]; 3) if the PS fails, e.g., due to a natural disaster, the whole system may break down. Therefore, in many important scenarios, such as swarms of unmanned aerial vehicles in a remote area [8] or in disaster response situations, a decentralized architecture may be more attractive, in which devices solve  $\{\mathbf{P}\}$  in a fully-decentralized fashion, without central coordination [9].

A renowned algorithm to solve  $\{\mathbf{P}\}$  in a fully-decentralized fashion is *Decentralized Gradient Descent* (DGD) [10], [11] and its stochastic gradient variant [12]: each node ( $i$ ) owns a local copy  $\mathbf{w}_i$  of the parameter vector (its *state*), and transmits it to its neighbors in the network; upon receiving its neighbors' states, it then updates  $\mathbf{w}_i$  as a weighted average of the received signals (the consensus signal  $\mathbf{c}_i$ ), followed by a local gradient step, illustrated here as non-stochastic for clarity,

$$\mathbf{w}_i \leftarrow \mathbf{c}_i - \eta \nabla f_i(\mathbf{w}_i), \text{ with } \mathbf{c}_i = \sum_{j=1}^N \omega_{i,j} \mathbf{w}_j. \quad \{\text{DGD}\}$$

Here,  $\omega_{i,j}$  are a set of non-negative, symmetric ( $\omega_{i,j} = \omega_{j,i}$ ) mixing weights, such that  $\sum_{j=1}^N \omega_{i,j} = 1$  ( $\omega_{i,j} = 0$  if  $i$  and  $j$  are not direct neighbors). Yet, the updates of  $\{\text{DGD}\}$  inherently assume communications over noise-free links (represented by a mesh network), and rely on a predetermined set of weights  $\omega$  to mix the incoming signals. In many practical scenarios, such as swarms of UAVs, the  $N$  nodes communicate over wireless links, subject to interference from concurrent transmissions, fading and noise, which can impede reliable communication. Mitigating these sources of signal degradation typically requires topology information to manage interference via transmission scheduling (e.g. TDMA/OFDMA), and the acquisition of channel state information (CSI) to compensate signal fluctuations and link outages caused by fading. Yet, executing these tasks may be challenging without centralized coordination, and a source of severe overhead, especially in densely-deployed networks with many devices.

### A. Novelty and Contributions

Addressing these challenges necessitates the design of decentralized optimization schemes tailored to wireless propagation environments. To meet this objective, in this paper we introduce a *Non-Coherent (NC)-Over-the-Air (OTA)-DGD* algorithm. Unlike conventional DGD approaches aiming at receiving individual copies of the neighbors' states (e.g., via TDMA scheduling), the key idea of NCOTA-DGD is to compute the consensus signal  $\mathbf{c}_i$  directly over the wireless channel, in line with over-the-air computing (AirComp) paradigms proposed in the FL setting [6], [13]–[17]. Nevertheless, prior AirComp approaches typically rely on *coherent* alignment of signals at a common base station, achieved via accurate CSI acquisition, channel inversion, and power control at the

N. Michelusi is with the School of Electrical, Computer and Energy Engineering, Arizona State University. Part of this work appeared at IEEE ICC'23 [1] and was accepted at IEEE ICASSP'24 [2].

This research has been funded in part by NSF under grant CNS-2129615.

transmitters. In a decentralized setting, this coherent alignment condition cannot be met because signals are broadcast to multiple receivers, each receiving through a different channel.

To address this challenge, we exploit a *noisy energy superposition property* of wireless channels. Nodes encode their local state  $\mathbf{w}_i$  into transmitted energy levels and transmit simultaneously using a randomized scheme for half-duplex operation. Leveraging the circularly symmetric nature of wireless channels, the received signal energy is, on average, the sum of individual transmitted signal energies scaled by their respective channel gains, akin to the consensus signal  $\mathbf{c}_i$ , but with channel gains acting as mixing weights. Introducing a suitable consensus stepsize mitigates energy fluctuations in the received signal (noise in the consensus estimate). The benefits of our approach over conventional DGD schemes implemented on mesh networks [18]–[20] are three-fold: 1) concurrent transmissions obviate the need for scheduling or inter-agent coordination, resulting in fast (albeit noisy) iterations and scalability in densely-deployed networks; 2) by leveraging intrinsic channel properties for signal mixing, explicit computation of mixing weights or topology information is unnecessary; 3) utilizing a non-coherent energy-based transmission and reception scheme eliminates the need for channel state information at transmitters or receivers.

Furthermore, we develop a novel analysis of DGD with noisy consensus and noisy gradients, for the class of strongly-convex problems. We prove that, by choosing the learning stepsize as  $\eta_k \propto 1/k$  and the consensus stepsize as  $\gamma_k \propto k^{-3/4}$  at the  $k$ th iteration, the expected squared distance between the local and globally optimum models vanishes with rate  $\mathcal{O}(1/\sqrt{k})$ . This result improves prior works [18], [19], exhibiting non-vanishing errors, and [21] using fixed stepsizes.

Lastly, we propose extensions to cover a wide range of fading models and frequency-selective channels, including static channels as a special case. Our numerical experiments focus on fashion-MNIST [22] image classification, formulated as regularized cross-entropy loss minimization. We demonstrate faster convergence compared to state-of-the-art algorithms, including quantized DGD [21], a device-to-device wireless implementation of DGD [18], and AirComp-based FL [6]. Notably, our approach excels in densely deployed networks with large number of learning devices.

### B. Related work

The study of distributed optimization algorithms to solve  $\{\mathbf{P}\}$  is vast and can be traced back to the seminal work [23]. While various works allow decentralized algorithms to operate over finite capacity channels, via compression [24]–[26] or quantization [27]–[30] of the transmitted signals, they rely on the presence of a mesh network for reliable, interference-free communications. This necessitates the use of transmission scheduling methods (e.g., TDMA) to manage interference. With the exception of [30], considering noise in the channel, they also assume error-free communications, hence do not account for the impact of noise and fading in wireless channels.

The works [31]–[33] consider the impact of unreliable communications, but rely on orthogonal transmissions, hence may scale poorly with respect to  $N$ . These schemes are not exempt from the issues outlined above.

Recently, there has been significant interest in the design of

schemes that leverage the waveform superposition properties of wireless channels via AirComp [34], first studied from an information-theoretic perspective in [35]. Most of these works are based on a centralized FL architecture with a base station acting as PS [6], [13]–[17], [36]. Yet, they rely on assumptions not easily applicable to decentralized settings:

- **CSI:** The works [6], [13]–[15] rely on accurate CSI at transmitters to enable channel inversion and ensure coherent alignment of the signals received at the PS. However, coherent alignment cannot be attained in decentralized settings, where transmitted signals are broadcast to all other devices, each receiving the signals through a different channel.
- **Scheduling overhead:** Centralized FL schemes typically require meticulous power control and device scheduling algorithms to enforce power constraints and ensure device participation. However, the ensuing signaling overhead, often presumed error-free or its impact not assessed, might not scale effectively to decentralized networks.
- **Massive-MIMO:** The work [16] overcomes the need for CSI at the transmitters by assuming a large number of antennas at the PS and by leveraging the channel hardening effect. However, edge devices (e.g., UAVs) with compact form factor may not have large number of antennas.
- **Noise-free downlink:** All these papers (except [15]) assume noise-free downlink. While reasonable for a PS with a typically larger power budget, this assumption may not hold under stringent power constraints of edge devices.

In contrast, the proposed scheme, NCOTA-DGD, does not require CSI (at neither transmitters nor receivers) and does not rely on large number of antennas, thanks to the use of non-coherent energy-based signaling strategies. NCOTA-DGD does not rely on power control or scheduling of devices, and is thus scalable to fully decentralized settings.

Key exceptions in the AirComp literature with star-based topology include [36], [37] (no CSI) and [38] (partial CSI). In [36], a centralized FL scheme is introduced with noise-free downlink channels. Gradient signals are encoded using random vector quantization [39] and transmitted via preamble-based random access. In this paper, we instead leverage an energy-based encoding strategy based on a representation of signals as a convex combination of codewords. Furthermore, the scheme developed in [39] relies on inversion of the average pathloss at the transmitters to ensure unbiased estimation of the global gradient at the PS, and on large number of antennas at the PS to achieve vanishing optimality error. In contrast, NCOTA-DGD achieves vanishing errors without relying on these assumptions, via a suitable processing of the received signals, and design of consensus and learning stepsizes for error mitigation. In [37], blind over-the-air computation (BlairComp) of nomographic functions over multiple access channels is addressed using a Wirtinger flow method. While [37] provides estimation error bounds for BlairComp, it does not ensure unbiased estimates, crucial for proving convergence of FL and DGD algorithms. The paper [38] focuses on over-the-air computation in the FL setting. It uses channel phase correction at the transmitters (partial CSI) to produce coherent alignment at the PS. However, as outlined earlier, coherent phase alignment cannot be achieved in a fully-decentralized setting with multiple receivers, hence the non-coherent energy

superposition technique developed in this paper.

Some recent works have developed algorithms for decentralized FL that are robust to wireless propagation impairments [18]–[20]. These algorithms mitigate interference by decomposing the network into smaller non-interfering subgraphs, via graph coloring techniques. In each subgraph, one device operates as the PS, which enables the use of techniques described earlier for centralized FL architectures, coupled with a suitable consensus enforcing step similar to {DGD}. However, these schemes rely on topology information for graph coloring, and may incur severe overhead to enable the acquisition of CSI at the transmitters, power control, and scheduling operations. These operations may not be scalable to fully-decentralized networks lacking a coordinator. In addition, these papers rely on prior knowledge of the mixing weights  $\omega$ , used to compute the consensus signal in {DGD}. Methods developed in [40] to estimate  $\omega$  rely on noise and interference-free links, and may further increase signaling overhead. In contrast, in this paper, we leverage the average pathloss as a proxy for mixing weights, eliminating the need for explicit knowledge thereof.

Finally, the works [41]–[44] proposed *semi-decentralized* FL architectures, where edge devices collaborate with their neighbors unable to form a reliable direct link with the PS. However, these works inherit similar challenges outlined earlier under both centralized and decentralized architectures. *C. Notation and Organization of the paper*

For a set  $S \subset \mathbb{R}^d$ , we denote its interior as  $\text{int}(S)$ , its boundary as  $\text{bd}(S)$ , and its convex hull as  $\text{conv}(S)$ . For matrix  $\mathbf{A}$ ,  $[\mathbf{A}]_{i,j}$  is its  $(i,j)$ th component,  $\mathbf{A}^\top$  its transpose,  $\mathbf{A}^H$  its complex conjugate transpose. Vectors are all defined in column form. For (column) vector  $\mathbf{a}$ ,  $[\mathbf{a}]_i$  is its  $i$ th component,  $\|\mathbf{a}\| = \sqrt{\mathbf{a}^H \mathbf{a}}$  its Euclidean norm. For a random vector  $\mathbf{a}$ , we define  $\|\mathbf{a}\|_{\mathbb{E}} \triangleq \sqrt{\mathbb{E}[\|\mathbf{a}\|^2]}$  ( $\|\mathbf{a}\|_{\mathbb{E}} = \|\mathbf{a}\|$  when  $\mathbf{a}$  is deterministic); we let  $\text{var}(\mathbf{a}) \triangleq \mathbb{E}[\|\mathbf{a}\|^2] - \|\mathbb{E}[\mathbf{a}]\|^2$  (variance) and  $\text{sdv}(\mathbf{a}) \triangleq \sqrt{\text{var}(\mathbf{a})}$  (standard deviation). We write  $\|\mathbf{a}\|_{\mathbb{E}|\mathcal{F}}$ ,  $\text{var}(\mathbf{a}|\mathcal{F})$  and  $\text{sdv}(\mathbf{a}|\mathcal{F})$  when the expectation is conditional on  $\mathcal{F}$ .  $\mathbf{a} \odot \mathbf{b}$  is the Hadamard (entry-wise) product of  $\mathbf{a}$  and  $\mathbf{b}$ . We define the following  $n$ -dimensional vectors/matrices: the  $m$ th standard basis vector  $\mathbf{e}_{n,m}$ , with  $m$ th component = 1, and 0 otherwise; the all ones and all zeros vectors  $\mathbf{1}_n$  and  $\mathbf{0}_n$ ; the  $n \times n$  identity matrix  $\mathbf{I}_n$ ; when clear from the context, we omit their dimension  $n$ .  $\mathbb{1}[A]$  is the indicator of event  $A$ .

The rest of this paper is organized as follows. In Secs. II–III, we present the system model and NCOTA-DGD. In Sec. IV, we delve into its convergence analysis, with proofs provided in the Appendix. In Sec. V, we present numerical results, followed by concluding remarks in Sec. VI. Supplementary details, including additional proofs and extended numerical results, are provided in the supplemental document.

## II. SYSTEM MODEL AND NCOTA-DGD

Consider  $N$  wirelessly-connected nodes solving {P} in a decentralized fashion. We divide time into frames of duration  $T$ . In this section, we consider a generic frame (iteration)  $k$ , and omit the dependence on  $k$ . In each iteration, we aim at emulating {DGD}, expressed in the equivalent form

$$\mathbf{w}_i \leftarrow \mathbf{w}_i + \gamma \mathbf{d}_i - \eta \nabla f_i(\mathbf{w}_i), \quad \text{with } \mathbf{d}_i = \sum_{j=1}^N \ell_{i,j}(\mathbf{w}_i - \mathbf{w}_j), \quad (1)$$

where  $\mathbf{d}_i$  is the *disagreement signal*,  $\ell_{i,j}$  are a set of Laplacian weights such that  $\ell_{i,j} = \ell_{j,i} \leq 0$  for  $i \neq j$ ,  $\ell_{i,i} = -\sum_{j \neq i} \ell_{i,j} > 0$ ,

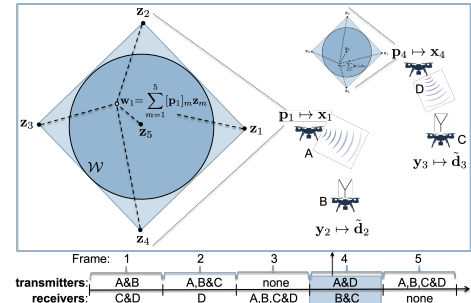


Fig. 1: Example of  $d=2$ -dimensional problem with  $N=4$  nodes. In frame  $k=4$ , nodes A and D encode their local optimization signal  $\mathbf{w}_i$  to a transmit signal  $\mathbf{x}_i$  (Eq. 3), and transmit simultaneously; receiving nodes C and D estimate the disagreement signal  $\tilde{\mathbf{d}}_i$  from their received signal  $\mathbf{y}_i$  (Eqs. 4–7).

and  $0 < \gamma \leq 1/\max_i \ell_{i,i}$ .<sup>1</sup> Note that  $\mathbf{w}_i + \gamma \mathbf{d}_i$  is equivalent to the consensus signal  $\mathbf{c}_i$  of {DGD}. To this end, node  $i$  maps its local optimization signal  $\mathbf{w}_i$  to an OFDM symbol  $\mathbf{x}_i$  using an *energy-based encoding procedure*, and transmits it over the wireless channel. It then estimates the *disagreement signal*,  $\tilde{\mathbf{d}}_i$  from the received signal  $\mathbf{y}_i$ ; finally, it updates  $\mathbf{w}_i$  by combining it with  $\tilde{\mathbf{d}}_i$ , followed by local gradient descent. Unlike prior DGD work, we assume lack of channel state and topology information at both transmitters and receivers, necessitating the use of *non-coherent energy estimation* methods. These steps are described next. An example is shown in Fig. 1.

We assume that the optimizer of {P} is known to lie in a closed, convex and bounded set  $\mathcal{W}$ . Thus,  $\mathbf{w}^* \in \mathcal{W}$ ,  $\mathbf{w}_i \in \mathcal{W}$ ,  $\forall i$ , and {P} is restricted within this set. For strongly-convex global functions  $F(\cdot)$  with strong-convexity parameter  $\mu$  (see Assumption 2),  $\mathcal{W}$  may be chosen as the  $d$ -dimensional sphere with radius  $\frac{1}{\mu} \|\nabla F(\mathbf{0})\|$ ,<sup>2</sup> computed at initialization.

*Energy-based encoding & transmission:* Let  $\mathcal{Z} = \{\mathbf{z}_m \in \mathbb{R}^d : m = 1, \dots, M\}$  be a codebook of  $M$  codewords such that  $\text{conv}(\mathcal{Z}) \supseteq \mathcal{W}$  (see Example 1 and Fig. 1).  $\mathcal{Z}$  is common knowledge among the nodes and remains fixed over iterates. Therefore, any  $\mathbf{w} \in \mathcal{W}$  may be represented as a convex combination of  $\mathcal{Z}$ . In other words, there exists a probability vector  $\mathbf{p} \in \mathbb{R}^M$  (i.e.,  $\mathbf{1}^\top \cdot \mathbf{p} = 1$ ,  $\mathbf{p} \geq \mathbf{0}$ ) such that

$$\mathbf{w} = \sum_{m=1}^M [\mathbf{p}]_m \mathbf{z}_m. \quad (2)$$

**Example 1** (Cross-polytope- $\phi$  (CP $\phi$ ) codebook). Let  $\mathcal{W} \equiv \{\mathbf{w} : \|\mathbf{w}\| \leq r\}$  ( $d$ -dimensional sphere of radius  $r$ ). Consider  $M=2d+1$   $d$ -dimensional codewords defined as  $\mathbf{z}_{2d+1} = \mathbf{0}$ ,

$$\mathbf{z}_m = \sqrt{d} \mathbf{e}_m, \quad \mathbf{z}_{d+m} = -\sqrt{d} \mathbf{e}_m, \quad \text{for } m = 1, \dots, d.$$

Then, for any  $\mathbf{w} \in \mathcal{W}$ , one can define the convex combination weights as  $[\mathbf{p}]_{2d+1} = 1 - \phi - \frac{1}{\sqrt{dr}} \|\mathbf{w}\|_1$ , and, for  $m=1, \dots, d$ ,

$$[\mathbf{p}]_m = \frac{1}{\sqrt{dr}} ([\mathbf{w}]_m)^+ + \frac{\phi}{2d}, \quad [\mathbf{p}]_{d+m} = \frac{1}{\sqrt{dr}} (-[\mathbf{w}]_m)^+ + \frac{\phi}{2d},$$

where  $(\cdot)^+ = \max\{\cdot, 0\}$ ,  $\phi \in [0, 1 - \frac{1}{\sqrt{dr}} \|\mathbf{w}\|_1]$ , and  $\|\cdot\|_1$  is the  $\ell_1$  norm. It is straightforward to see that  $[\mathbf{p}]_m \geq 0, \forall m$  and, since  $(x)^+ - (-x)^+ = x$ , (2) holds, so that  $\mathbf{p}$  defines the desired convex combination. The cross-polytope vector quantization of [39] is a special case with  $\phi = 1 - \frac{1}{\sqrt{dr}} \|\mathbf{w}\|_1$  and  $[\mathbf{p}]_{2d+1} = 0$ .

Given  $\mathbf{w}_i$  and the associated probability vector  $\mathbf{p}_i$ , node  $i$  generates the transmit signal  $\mathbf{x}_i$  as follows. We assume frequency-selective channels with non-negligible propagation

<sup>1</sup>(1) maps to {DGD} with  $\omega_{i,j} = -\gamma \ell_{i,j}$  for  $i \neq j$ , and  $\omega_{i,i} = 1 - \gamma \ell_{i,i}$ .

<sup>2</sup>Strong convexity and the optimality condition  $\nabla F(\mathbf{w}^*) = \mathbf{0}$  imply  $\|\nabla F(\mathbf{0})\| = \|\nabla F(\mathbf{0}) - \nabla F(\mathbf{w}^*)\| \geq \mu \|\mathbf{0} - \mathbf{w}^*\|$ , hence  $\|\mathbf{w}^*\| \leq \|\nabla F(\mathbf{0})\|/\mu$ .



delays between node pairs, hence the use of OFDM signaling. For clarity, we assume that each transmission is structured into one OFDM symbol with  $M$  subcarriers (matching the codebook size  $|\mathcal{Z}|$ ). We will extend this configuration to a generic number of subcarriers and/or OFDM symbols in Sec. III. Node  $i$  then maps  $\mathbf{p}_i$  to the transmit signal

$$[\mathbf{x}_i]_m = \sqrt{E \cdot M} \sqrt{[\mathbf{p}_i]_m}, \quad \forall m = 1, \dots, M, \quad (3)$$

on the  $m$ th subcarrier, with energy per sample  $E$ . In other words,  $\mathbf{p}_i$  encodes the energies allocated on each subcarrier.

Noisy energy superposition property: To accommodate half-duplex constraints, each node transmits in the current frame with probability  $p_{\text{tx}}$ , indicated as  $\chi_i=1$  for node  $i$ , and receives otherwise ( $\chi_i = 0$ ). These transmission decisions are independent over iterations  $k$  and across nodes. Let  $\mathbf{h}_{i,j} \in \mathbb{C}^M$  be the frequency-domain channel vector between transmitter  $j$  and receiver  $i$ , so that  $[\mathbf{h}_{i,j}]_m$  is the channel in the  $m$ th subcarrier. Then, node  $i$  receives

$$\mathbf{y}_i = (1 - \chi_i) \left[ \sum_{j \neq i} \chi_j \mathbf{h}_{i,j} \odot \mathbf{x}_j + \mathbf{n}_i \right], \quad (4)$$

where  $\mathbf{n}_i \sim \mathcal{CN}(\mathbf{0}, N_0 \mathbf{I})$  is AWGN noise with variance  $N_0$ . Note that no signal is received ( $\mathbf{y}_i = \mathbf{0}$ ) if node  $i$  transmits, due to half-duplex constraints. Then, it computes the energies

$$r_{i,m} = (1 - \chi_i) \frac{|[\mathbf{y}_i]_m|^2 - N_0}{p_{\text{tx}}(1 - p_{\text{tx}})EM}, \quad \forall m = 1, \dots, M, \quad (5)$$

with  $r_{i,m} = 0$  if it transmits. In this section, we assume Rayleigh fading channels (generalized to a broad class of channel models in Sec. III), independent across  $i, j$  and iterations  $k$ , so that  $[\mathbf{h}_{i,j}]_m \sim \mathcal{CN}(0, \Lambda_{i,j}), \forall m$  with average channel gain  $\Lambda_{i,j}$  ( $=\Lambda_{j,i}$  from channel reciprocity). Then, taking the expectation over noise, Rayleigh fading, and random transmission decision ( $\mathbb{P}(\chi_j = 1) = p_{\text{tx}}$ ), conditional on the probability vectors  $\mathbf{p}_j$ , one obtains

$$\mathbb{E}[r_{i,m}] = \sum_{j \neq i} \mathbb{E}[|[\mathbf{h}_{i,j}]_m|^2] [\mathbf{p}_j]_m = \sum_{j \neq i} \Lambda_{i,j} [\mathbf{p}_j]_m. \quad (6)$$

Hence,  $r_{i,m}$  represents an unbiased estimate of the sum of the convex combination weights, weighted by their channel gains. This *energy superposition property* is key to estimating the disagreement signal of (1), discussed next. Yet, it holds only in expectation:  $r_{i,m}$  exhibits fluctuations around its mean. The analysis of how these fluctuations impact convergence and are mitigated via a suitable stepsize design is conducted in Sec. IV.

Disagreement signal estimation: Node  $i$  then computes

$$\tilde{\mathbf{d}}_i = \sum_{m=1}^M r_{i,m} (\mathbf{z}_m - \mathbf{w}_i). \quad (7)$$

Note that, if node  $i$  transmits, then  $r_{i,m} = 0$  and  $\tilde{\mathbf{d}}_i = \mathbf{0}$ . Using (6) and (2), it is straightforward to show that

$$\mathbb{E}[\tilde{\mathbf{d}}_i] = \sum_{j \neq i} \Lambda_{i,j} (\mathbf{w}_j - \mathbf{w}_i) = \sum_{j=1}^N \ell_{i,j} (\mathbf{w}_i - \mathbf{w}_j), \quad (8)$$

where in the last step we defined the Laplacian weights  $\ell_{i,j} = -\Lambda_{i,j}$  and  $\ell_{i,i} = \sum_{j \neq i} \Lambda_{i,j}$ . Hence,  $\tilde{\mathbf{d}}_i$  is an unbiased estimate of the disagreement signal, with Laplacian weights

dictated by the channel gains  $\Lambda_{i,j}$ . They satisfy  $\ell_{i,j} \leq 0, \forall i \neq j$  and  $\ell_{i,j} = \ell_{j,i}$  (channel reciprocity). Hence,  $[\mathbf{L}]_{i,j} = \ell_{i,j}$  is a symmetric Laplacian matrix with  $\mathbf{L} \cdot \mathbf{1} = \mathbf{0}$ , induced by the large-scale propagation conditions. Yet, unlike (1), no explicit knowledge of  $\mathbf{L}$  is required: rather, the channel conditions are leveraged to mix the signals. The property (8) will be exploited in the next step to emulate the updates in (1).

Local optimization state update: During the frame, node  $i$  computes an unbiased stochastic gradient  $\mathbf{g}_i$ , with  $\mathbb{E}[\mathbf{g}_i | \mathbf{w}_i] = \nabla f_i(\mathbf{w}_i)$ . It then updates  $\mathbf{w}_i$  as

$$\mathbf{w}_i \leftarrow \Pi[\mathbf{w}_i + \gamma \tilde{\mathbf{d}}_i - \eta \mathbf{g}_i], \quad (9)$$

where  $\Pi[\mathbf{a}]$  is a projection operator,

$$\Pi[\mathbf{a}] = \arg \min_{\mathbf{w} \in \mathcal{W}} \|\mathbf{w} - \mathbf{a}\|,$$

restricting the algorithm within the set  $\mathcal{W}$ , so that  $\mathbf{w}_i \in \mathcal{W}, \forall i$ .  $\gamma, \eta > 0$  are (possibly, time-varying) *consensus* and *learning* stepsizes, respectively: the former controls information diffusion and mitigates signal fluctuations in the disagreement signal estimation; the latter regulates the magnitude of gradient steps, hence the learning progress. As detailed in Sec. IV, their design is crucial to balancing these competing objectives.

These steps are repeated in frame  $k+1$  with the new local optimization variable  $\mathbf{w}_i$ , and so on. Overall, NCOTA-DGD expressed in (9) can thus be interpreted as a projected DGD with noisy consensus and noisy gradients.

### III. GENERALIZATIONS

#### A. More general frame structure

More generally, a frame is constituted of  $O$  OFDM symbols, each with  $SC$  subcarriers, defining  $Q = O \times SC \geq M$  resource units. Let  $q \in \{1, \dots, Q\} \equiv \mathcal{Q}$  be the  $q$ th resource unit, on a certain OFDM symbol and subcarrier. Each component of the vector  $\mathbf{p}_i$  is then mapped to a set of  $M$  orthogonal sequences  $\{\mathbf{u}_m \in \mathbb{C}^Q : m = 1, \dots, M\}$ , defined on these resource units as

$$\mathbf{u}_m \triangleq \sqrt{Q/R_m} \sum_{q \in \mathcal{R}_m} \mathbf{e}_{Q,q}. \quad (10)$$

Here,  $\mathcal{R}_m \subset \mathcal{Q}$  is the set of  $R_m = |\mathcal{R}_m|$  resource units allocated to the  $m$ th sequence, defining a partition of  $\mathcal{Q}$  into  $M$  sets. Hence, the transmit signal is defined as

$$\mathbf{x}_i = \sqrt{E} \cdot \sum_{m=1}^M \sqrt{[\mathbf{p}_i]_m} \cdot \mathbf{u}_m,$$

so that  $[\mathbf{p}_i]_m$  scales the energy allocated on the  $m$ th sequence  $\mathbf{u}_m$ . With  $\mathbf{x}_i$  thus defined, the signal received by node  $i$  is given as in (4). Node  $i$  then computes the  $M$  energy signals

$$r_{i,m} = (1 - \chi_i) \sum_{q \in \mathcal{R}_m} \frac{|[\mathbf{y}_i]_q|^2 - N_0}{p_{\text{tx}}(1 - p_{\text{tx}})EQ}, \quad (11)$$

yielding (3)-(5) as a special case with  $Q=M$  and  $\mathcal{R}_m \equiv \{m\}$ . The signal  $r_{i,m}$  in (11) aggregates energies across the resource units  $\mathcal{R}_m$  allocated on the  $m$ th component, rather than a single subcarrier in (5). Taking the expectation with respect to noise, Rayleigh fading channels with  $\mathbb{E}[|[\mathbf{h}_{i,j}]_q|^2] = \Lambda_{i,j}$ , and random transmissions, we find  $\mathbb{E}[r_{i,m}] = \sum_{j \neq i} \Lambda_{i,j} [\mathbf{p}_j]_m$  as in (6), so that (8) still holds.

### B. Broad class of channel models

The unbiasedness of  $\tilde{\mathbf{d}}_i$  in (8) is key to proving convergence in Sec. IV, but it does not hold under more general channel models than those considered in Sec. II. For instance, with static channels, in which  $\mathbf{h}_{i,j}$  remains fixed over iterations  $k$ ,

$$\begin{aligned} \mathbb{E}[r_{i,m}] &= \sum_{j \neq i} \frac{1}{R_m} \sum_{q \in \mathcal{R}_m} |[\mathbf{h}_{i,j}]_q|^2 [\mathbf{p}_j]_m \\ &+ 2p_{\text{tx}} \sum_{j,j' \neq i: j' < j} \frac{1}{R_m} \sum_{q \in \mathcal{R}_m} \text{re}([\mathbf{h}_{i,j}]_q [\mathbf{h}_{i,j'}]_q^*) \sqrt{[\mathbf{p}_j]_m [\mathbf{p}_{j'}]_m}. \end{aligned} \quad (12)$$

Compared to (6): 1) each component of  $\mathbf{p}_j$  experiences a different average channel gain,  $\frac{1}{R_m} \sum_{q \in \mathcal{R}_m} |[\mathbf{h}_{i,j}]_q|^2$  for the  $m$ th component, instead of a common  $\Lambda_{i,j}$ ; and 2) the cross-product terms  $\text{re}([\mathbf{h}_{i,j}]_q [\mathbf{h}_{i,j'}]_q^*)$  do not vanish. As a result, a bias term appears, that accumulates over time and leads to loss of the convergence properties. To recover the unbiasedness of  $\tilde{\mathbf{d}}_i$ , we introduce two mechanisms under a broad class of channels, including Rayleigh fading and static as special cases.

**Assumption 1.** *The channels  $\mathbf{h}_{i,j}$  are i.i.d. over iterations  $k$ .<sup>3</sup> We define the average gain across  $\mathcal{R}_m$  as*

$$\mathbb{E} \left[ \frac{1}{R_m} \sum_{q \in \mathcal{R}_m} |[\mathbf{h}_{i,j}]_q|^2 \right] \triangleq \Lambda_{i,j}^{(m)},$$

and further across  $m$  as  $\Lambda_{i,j} \triangleq \frac{1}{M} \sum_{m=0}^{M-1} \Lambda_{i,j}^{(m)}$ .

*Random phase shift:* each transmitter applies a random phase shift to the transmit signal, uniform in  $[0, 2\pi]$ , i.i.d. over time and across nodes, and i.i.d. across resource units within the same set  $\mathcal{R}_m$ . Let  $[\theta_j]_q$  be the phase shift applied to the  $q$ th resource unit by node  $j$ . Then, the combined channel  $\tilde{\mathbf{h}}_{i,j} = e^{j\theta_j} \odot \mathbf{h}_{i,j}$  between transmitter  $j$  and receiver  $i$  becomes circularly symmetric, yielding  $\mathbb{E}[\text{re}([\tilde{\mathbf{h}}_{i,j}]_q [\tilde{\mathbf{h}}_{i,j'}]_q^*)] = 0, \forall j \neq j'$ , upon taking the expectation on  $\theta_j$ . Therefore, the cross product terms in (12) vanish under a random phase shift.

*Coordinated circular subcarrier shift:* each transmitter applies a shift  $\varsigma$  to the mapping of signal components to resource units, i.e.,  $[\mathbf{p}_i]_m$  is mapped to the resource units in the set  $\mathcal{R}_{m \oplus \varsigma}$ ;<sup>4</sup>  $\varsigma$  is chosen uniformly at random in  $\mathcal{M} \equiv \{0, \dots, M-1\}$ , i.i.d. over time, and identical across devices (e.g., a pseudo-random sequence with a common seed). Thanks to this mechanism, on average, each signal component undergoes all resource units, and experiences the same average channel gain  $\Lambda_{i,j}$ .

Combining these two mechanisms, the transmit signal is

$$\mathbf{x}_i = \sqrt{E} \cdot e^{j\theta_i} \odot \sum_{m=1}^M \sqrt{[\mathbf{p}_i]_m} \cdot \mathbf{u}_{m \oplus \varsigma}. \quad (13)$$

Upon receiving  $\mathbf{y}_i$  as in (4), node  $i$  maps the signal received on shifted resource units  $\mathcal{R}_{m \oplus \varsigma}$  to  $r_{i,m}$ , hence we modify (11) as

$$r_{i,m} = (1 - \chi_i) \sum_{q \in \mathcal{R}_{m \oplus \varsigma}} \frac{|[\mathbf{y}_i]_q|^2 - N_0}{p_{\text{tx}}(1 - p_{\text{tx}})EQ}. \quad (14)$$

$\tilde{\mathbf{d}}_i$  is then computed as in (7), and the local model update follows (9). Taking the expectation of  $r_{i,m}$  with respect to the phase shifts, random transmissions, noise and channels, conditional on the subcarrier shift  $\varsigma$ , one obtains

<sup>3</sup>Please note: static channels can be interpreted as a degenerate i.i.d. process in which  $\mathbf{h}_{i,j}$  takes a deterministic value, with probability 1.

<sup>4</sup>Here,  $m \oplus \varsigma = 1 + \text{mod}(m-1+\varsigma, M)$  is the sum modulo  $M$

$\mathbb{E}[r_{i,m}|\varsigma] = \sum_{j \neq i} \Lambda_{i,j}^{(m \oplus \varsigma)} [\mathbf{p}_j]_m, \forall m = 1, \dots, M$ , i.e., the cross-product term in (12) vanishes, thanks to the circular symmetry of the equivalent channels. Further taking the expectation with respect to  $\varsigma \sim \text{uniform}(\mathcal{M})$  yields

$\mathbb{E}[r_{i,m}] = \sum_{j \neq i} \frac{1}{M} \sum_{m'=1}^M \Lambda_{i,j}^{(m')}$   $[\mathbf{p}_j]_m = \sum_{j \neq i} \Lambda_{i,j} [\mathbf{p}_j]_m$ , since  $m \oplus \varsigma$  becomes uniform in  $1, \dots, M$ . Overall, each component  $m$  of the signal experiences the same average channel gain  $\Lambda_{i,j}$ . This property yields an unbiased estimate of the disagreement signal, as in (8), hence the convergence analysis of Sec. IV readily applies.

Therein, the convergence is dictated by the variance of the estimation error  $\tilde{\mathbf{d}}_i - \mathbb{E}[\tilde{\mathbf{d}}_i]$ , bounded in the next lemma. It shows the impact of: the variation of  $|[\mathbf{h}_{i,j}]_q|^2$  around the average channel gain (averaged across resource units)  $\Lambda_{i,j}$ , captured by the term  $\vartheta$ ; the variation of  $\hat{\lambda}_{i,j}^{(m)}$  (sample average channel gain across  $\mathcal{R}_m$ ) around  $\Lambda_{i,j}$ , captured by the term  $\varsigma$ ; the maximum sum gain ( $\Lambda^*$ ). Based on this bound, the lemma also provides the optimal design of the transmission probability  $p_{\text{tx}}$  (proof in the supplemental document).

**Lemma 1.** *Consider channels satisfying Assumption 1. Furthermore, assume the resource units are evenly allocated among  $m = 1, \dots, M$ , i.e.,  $|R_m - Q/M| < 1, \forall m$ . Let:*

$$\vartheta \triangleq \max_{i,j \neq i} \frac{1}{\Lambda_{i,j}} \left( \frac{1}{Q} \sum_{q=1}^Q \mathbb{E}[ (|[\mathbf{h}_{i,j}]_q|^2 - \Lambda_{i,j})^2 ] \right)^{1/2}, \quad (15)$$

$$\varsigma \triangleq \max_{i,j \neq i} \frac{1}{\Lambda_{i,j}} \left( \frac{1}{M} \sum_{m=1}^M \mathbb{E}[ (\hat{\lambda}_{i,j}^{(m)} - \Lambda_{i,j})^2 ] \right)^{1/2}, \quad (16)$$

$$\Lambda^* \triangleq \max_i \sum_{j \neq i} \Lambda_{i,j}, \quad (17)$$

where  $\hat{\lambda}_{i,j}^{(m)} = \frac{1}{R_m} \sum_{q \in \mathcal{R}_m} |[\mathbf{h}_{i,j}]_q|^2$  is the sample average channel gain across the resource units in the set  $\mathcal{R}_m$ . Then,  $\frac{1}{N} \sum_{i=1}^N \text{var}(\tilde{\mathbf{d}}_i) \leq \Sigma^{(1)} \triangleq \max_{\mathbf{z}, \mathbf{z}' \in \mathcal{Z}} \|\mathbf{z} - \mathbf{z}'\|^2$

$\times \frac{1}{1-p_{\text{tx}}} \left[ \frac{\sqrt{M}}{\sqrt{Q}} \sqrt{2(1+2\vartheta^2)} \Lambda^* + \frac{\sqrt{1+\varsigma^2}}{\sqrt{p_{\text{tx}}}} \Lambda^* + \frac{\sqrt{M}}{\sqrt{Q}} \frac{N_0}{E p_{\text{tx}}} \right]^2$ . The value of the transmission probability  $p_{\text{tx}}$  minimizing this bound is the unique solution in  $(0, 1)$  of  $\sqrt{2(1+2\vartheta^2)} \Lambda^* p_{\text{tx}}^{3/2} + \frac{\sqrt{Q}}{\sqrt{M}} \sqrt{1+\varsigma^2} \Lambda^* (2p_{\text{tx}} - 1) + \frac{N_0}{E} \frac{3p_{\text{tx}} - 2}{\sqrt{p_{\text{tx}}}} = 0$ .

For Rayleigh fading channels discussed in Sec. II, and assuming the channel gains are independent across  $q \in \mathcal{R}_m$  (achieved by spacing apart the resource units belonging to the same  $\mathcal{R}_m$  by more than the channel's coherence bandwidth) we find  $\vartheta=1$  and  $\varsigma \approx \sqrt{M/Q}$ . Algorithm 1 outlines the steps of NCOTA-DGD described in this section. Each OFDM symbol, with a communication bandwidth  $W_{\text{tot}}$ , has a duration  $T_{\text{ofdm}} = (\text{SC} + \text{CP})/W_{\text{tot}}$  (SC subcarriers; cyclic prefix length CP). With  $O$  OFDM symbols required to transmit the  $Q = O \cdot \text{SC}$ -dimensional signal  $\mathbf{x}_i$ , the frame duration is

$$T = O \cdot T_{\text{ofdm}} = W_{\text{tot}}^{-1} \cdot O \cdot (\text{SC} + \text{CP}), \quad (18)$$

irrespective of network size  $N$ . This highlights the scalability of NCOTA-DGD over large wireless networks, unlike a TDMA scheme where  $T$  grows linearly with  $N$ .

## IV. CONVERGENCE ANALYSIS

In this section, we study the convergence of Algorithm 1 as it progresses over multiple iterations. Hence, we express the

---

**Algorithm 1** NCOTA-DGD iteration

- 1: **procedure** (at node  $i$ , given  $\mathbf{w}_i$ , circular shift  $\varsigma$ , stepsizes  $\eta, \gamma$ )
  - 2: **Computation** (in parallel with communication): compute an unbiased stochastic gradient  $\mathbf{g}_i$  based on the local  $f_i$  at  $\mathbf{w}_i$ ;
  - 3: **Random transmission decision** select  $\chi_i = 1$  with probability  $p_{\text{tx}}$ ,  $\chi_i = 0$  otherwise;
  - 4: **Communication – if transmission** ( $\chi_i = 1$ ):
  - 5:   → Compute the convex combination  $\mathbf{p}_i$  (see Example 1);
  - 6:   → Generate random phase  $\theta_i$  and transmit signal  $\mathbf{x}_i$  via (13);
  - 7:   → Map  $\mathbf{x}_i$  to  $O$  OFDM symbols, each with SC subcarriers;
  - 8:   → Set  $\tilde{\mathbf{d}}_i = \mathbf{0}$ ;
  - 9: **Communication – if reception** ( $\chi_i = 0$ ):
  - 10:   → Receive  $\mathbf{y}_i$  (see (4));
  - 11:   → Compute the  $M$  energy signals via (14);
  - 12:   → Estimate the disagreement signal  $\tilde{\mathbf{d}}_i$  via (7);
  - 13: **DGD update:**  $\mathbf{w}_i \leftarrow \Pi[\mathbf{w}_i + \gamma\mathbf{d}_i - \eta\mathbf{g}_i]$  as in (9).
  - 14: **end procedure** repeat in the next iteration.
- 

dependence of the signals and stepsizes on the iteration index  $k$ . Due to randomness of noise, fading, random transmissions, phase and circular subcarrier shifts at transmitters, Algorithm 1 induces a stochastic process. We denote by  $\mathcal{F}_k$  the  $\sigma$ -algebra generated by the signals up to frame  $k-1$ , along with  $\mathbf{w}_{i,k}$ ,  $\forall i$ . In essence, when taking expectations conditioned on  $\mathcal{F}_k$ , we consider the randomness generated during the  $k$ th iteration, conditional on the signals available at the start of that iteration.

To analyze NCOTA-DGD, we first stack its updates over the network, and make the error terms explicit (Sec. IV.A). We then introduce assumptions and definitions used in the analysis, commonly adopted in prior work (Sec. IV.B). We present the main convergence result in Sec. IV.C, then specialize it to constant (Sec. IV.D). and decreasing (Sec. IV.E) stepsizes.

#### A. Equivalent representation of NCOTA-DGD

We use lowercase variables for node-specific signals ( $\mathbf{a}_i$  for node  $i$ ) and uppercase variables for their concatenation over the network ( $Nd$ -dimensional vector  $\mathbf{A} = [\mathbf{a}_1^\top, \mathbf{a}_2^\top, \dots, \mathbf{a}_N^\top]^\top$ ). Thus,  $\mathbf{W}_k$ ,  $\mathbf{G}_k$ , and  $\tilde{\mathbf{D}}_k$  concatenate the  $\mathbf{w}_{i,k}$ ,  $\mathbf{g}_{i,k}$ , and  $\tilde{\mathbf{d}}_{i,k}$  signals at iteration  $k$ . Additionally, we define  $\mathbf{W}^* = \mathbf{1}_N \otimes \mathbf{w}^*$  as the concatenation of  $\mathbf{w}^* = \arg \min_{\mathbf{w} \in \mathbb{R}^d} F(\mathbf{w})$ . Let

$$f(\mathbf{W}) = \sum_{i=1}^N f_i(\mathbf{w}_i). \quad (19)$$

Noting that  $\nabla f(\mathbf{W}) = [\nabla f_1(\mathbf{w}_1)^\top, \nabla f_2(\mathbf{w}_2)^\top, \dots, \nabla f_N(\mathbf{w}_N)^\top]^\top$ , we can then rewrite the update (9) as

$$\mathbf{W}_{k+1} = \Pi^N[\mathbf{W}_k + \gamma_k \tilde{\mathbf{D}}_k - \eta_k \mathbf{G}_k], \quad (20)$$

where  $\mathbb{E}[\mathbf{G}_k | \mathcal{F}_k] = \nabla f(\mathbf{W}_k)$  (unbiased gradient estimate) and  $\Pi^N[\cdot]$  is a projection onto  $\mathcal{W}^N$ . We rewrite it by isolating the errors in the disagreement signal estimation due to fading, noise, phase and circular subcarrier shifts, and random transmissions ( $\epsilon_k^{(1)}$ ), and in the stochastic gradients ( $\epsilon_k^{(2)}$ ). Namely,

$$\epsilon_k^{(1)} = \tilde{\mathbf{D}}_k - \mathbb{E}[\tilde{\mathbf{D}}_k | \mathcal{F}_k], \quad \epsilon_k^{(2)} = \mathbf{G}_k - \nabla f(\mathbf{W}_k).$$

By definition,  $\mathbb{E}[\epsilon_k^{(1)} | \mathcal{F}_k] = \mathbb{E}[\epsilon_k^{(2)} | \mathcal{F}_k] = \mathbf{0}$ . Letting  $\hat{\mathbf{L}} = \mathbf{L} \otimes \mathbf{I}_d$ , we then rewrite (20) in the equivalent form  $\mathbf{W}_{k+1}$

$$= \Pi^N \left[ \underbrace{(\mathbf{I} - \gamma_k \hat{\mathbf{L}}) \mathbf{W}_k - \eta_k \nabla f(\mathbf{W}_k)}_{(a)} + \underbrace{\gamma_k \epsilon_k^{(1)} - \eta_k \epsilon_k^{(2)}}_{(b)} \right], \quad (21)$$

where  $\mathbb{E}[\tilde{\mathbf{D}}_k | \mathcal{F}_k] = -\hat{\mathbf{L}} \mathbf{W}_k$  is obtained by concatenating

$\mathbb{E}[\tilde{\mathbf{d}}_{i,k} | \mathcal{F}_k]$ , given by (8). The term (a) specializes to the standard DGD update shown in (1) when  $\gamma_k = \gamma, \forall k$ ; the term (b) (referred to as the "noise" in the remainder), instead, captures the various sources of randomness. Following an approach similar to [11] for the analysis of DGD (therein, with fixed stepsize), we interpret the term (a) as a gradient descent update with stepsize  $\eta_k$ , based on the Lyapunov function

$$G_k(\mathbf{W}) \triangleq f(\mathbf{W}) + \frac{\gamma_k}{2\eta_k} \mathbf{W}^\top \cdot \hat{\mathbf{L}} \cdot \mathbf{W}.$$

Notably, the quadratic term in  $G_k$  enforces consensus in the network (in fact, it equals zero when  $\mathbf{w}_i = \mathbf{w}_j, \forall i, j$ ). Note that  $G_k$  is time-varying due to  $k$ -dependent stepsizes, thus generalizing [11] employing a fixed stepsize (hence a time-invariant  $G$ ). We can then express (21) compactly as

$$\mathbf{W}_{k+1} = \Pi^N[\mathbf{W}_k - \eta_k \nabla G_k(\mathbf{W}_k) + \gamma_k \epsilon_k^{(1)} - \eta_k \epsilon_k^{(2)}]. \quad (22)$$

#### B. Assumptions and Definitions

We study the convergence of NCOTA-DGD under standard assumptions commonly adopted in prior work, e.g., [18], [19].

**Assumption 2.** All  $f_i(\mathbf{w})$  are  $\mu$ -strongly convex,  $L$ -smooth.

A direct consequence is that the global  $F$  in  $\{\mathcal{P}\}$  and  $f$  in (19) are also  $\mu$ -strongly convex and  $L$ -smooth.

**Assumption 3.**  $\mathbf{w}^* \in \text{int}(\mathcal{W})$ , hence its distance from the boundary of  $\mathcal{W}$  satisfies  $\zeta \triangleq \min_{\mathbf{w} \in \text{bd}(\mathcal{W})} \|\mathbf{w} - \mathbf{w}^*\| > 0$ .<sup>5</sup>

As discussed after (8),  $\mathbf{L}$  is a symmetric Laplacian matrix with  $\mathbf{L} \cdot \mathbf{1} = \mathbf{0}$ , hence it is semidefinite positive with eigenvalues  $0 = \rho_1 \leq \rho_2 \leq \dots \leq \rho_N$ . We further assume that the large scale propagation conditions define a connected graph, yielding a strictly-positive algebraic connectivity  $\rho_2$  [45]:

**Assumption 4** (Algebraic connectivity of  $\mathbf{L}$ ).  $\rho_2 > 0$ .

Finally, we make the following assumption on  $\epsilon_k^{(1)}$  and  $\epsilon_k^{(2)}$ .

**Assumption 5.** There exist  $\Sigma^{(1)}, \Sigma^{(2)} \geq 0$  such that

$$\frac{1}{N} \mathbb{E}[\|\epsilon_k^{(1)}\|^2 | \mathcal{F}_k] \leq \Sigma^{(1)}, \quad \frac{1}{N} \mathbb{E}[\|\epsilon_k^{(2)}\|^2 | \mathcal{F}_k] \leq \Sigma^{(2)}.$$

Closed-form expressions are given in Lemma 1 for  $\Sigma^{(1)}$ ,<sup>6</sup> and in Appendix A for  $\Sigma^{(2)}$ , under minibatch gradients.

Since  $\mathcal{W}$  is bounded, its diameter is as well, defined below.

**Definition 1** (diameter of  $\mathcal{W}$ ).  $\text{dm}(\mathcal{W}) \triangleq \max_{\mathbf{w}, \mathbf{w}' \in \mathcal{W}} \|\mathbf{w} - \mathbf{w}'\|$ .

In Example 1,  $\text{dm}(\mathcal{W}) = 2r$ . Lastly, we define the gradient divergence at the global optimum  $\mathbf{w}^*$  (similar to [46]).

**Definition 2** (gradient divergence).  $\nabla^* \triangleq \max_i \|\nabla f_i(\mathbf{w}^*)\|$ .

#### C. Main convergence results

We restrict our analysis to  $k \geq \bar{k}$  under a suitable iteration index  $\bar{k}$  (to be defined later). It represents a regime in which stepsizes become sufficiently small to satisfy certain conditions stated in Theorem 1.<sup>7</sup> The proof of [21] considers fixed stepsizes and lacks a projection operator. Hence, its analysis

<sup>5</sup>The analysis may be relaxed to the case when  $\mathbf{w}^*$  lies on the boundary of  $\mathcal{W}$  ( $\zeta = 0$ ), but it yields looser convergence results.

<sup>6</sup>Note that  $\frac{1}{N} \mathbb{E}[\|\epsilon_k^{(1)}\|^2 | \mathcal{F}_k] = \frac{1}{N} \sum_{i=1}^N \text{var}(\tilde{\mathbf{d}}_i | \mathcal{F}_k)$ .

<sup>7</sup>For  $k < \bar{k}$ , one can simply bound  $\|\mathbf{w}_{i,k} - \mathbf{w}^*\| \leq \text{dm}(\mathcal{W})$ .

cannot be readily extended to the setup of this paper, calling for a new line of analysis presented herein. The main idea is to decompose the error between the local optimization variables  $\mathbf{W}_k$  and the global optimum  $\mathbf{W}^*$  into: {1} the error between  $\mathbf{W}_k$  and the *noise-free dynamics*  $\tilde{\mathbf{W}}_k$  (obtained by setting the term  $b$  in (21) equal to 0), defined by the updates  $\tilde{\mathbf{W}}_{\bar{k}} = \mathbf{W}_{\bar{k}}$ ,

$$\tilde{\mathbf{W}}_{k+1} = \Pi^N[\tilde{\mathbf{W}}_k - \eta_k \nabla G_k(\tilde{\mathbf{W}}_k)], \quad \forall k \geq \bar{k}; \quad (23)$$

{2} the error between  $\tilde{\mathbf{W}}_k$  and the minimizer of the *time-varying* Lyapunov function  $G_k$ , defined at iteration  $k$  as

$$\mathbf{W}_k^* = \arg \min_{\mathbf{W} \in \mathcal{W}^N} G_k(\mathbf{W}); \quad (24)$$

and {3} the error between  $\mathbf{W}_k^*$  and  $\mathbf{W}^*$ . Accordingly,

$$\begin{aligned} & \left( \mathbb{E} \left[ \sum \| \mathbf{w}_{i,k} - \mathbf{w}^* \|^2 \right] \right)^{1/2} = \| \mathbf{W}_k - \mathbf{W}^* \|_{\mathbb{E}} \quad (25) \\ & = \| (\tilde{\mathbf{W}}_k - \tilde{\mathbf{W}}_k) + (\tilde{\mathbf{W}}_k - \mathbf{W}_k^*) + (\mathbf{W}_k^* - \mathbf{W}^*) \|_{\mathbb{E}} \\ & \leq \| \mathbf{W}_k - \tilde{\mathbf{W}}_k \|_{\mathbb{E}} + \| \tilde{\mathbf{W}}_k - \mathbf{W}_k^* \|_{\mathbb{E}} + \| \mathbf{W}_k^* - \mathbf{W}^* \|, \quad (26) \end{aligned}$$

where the last step follows from Minkowski inequality [47, Lemma 14.10]. These terms are individually bounded in Theorem 1. A significant challenge in proving Theorem 1, in contrast to [21], stems from the time-varying behavior of  $G_k$ , caused by the use of time-varying stepsizes: in step {2}, one must tightly bound the *tracking error* associated with the changes in the  $G_k$ -minimizer  $\mathbf{W}_k^*$  over  $k$ . This issues is absent when using constant stepsizes as in [21].

**Theorem 1.** Assume  $\forall k \geq \bar{k}$ : **C1**:  $\eta_k(\mu+L) + \gamma_k \rho_N \leq 2$ ;  
**C2**:  $\frac{\eta_k}{\gamma_k} \leq \frac{\zeta \cdot \mu \rho_2}{\sqrt{N} \nabla^* L}$ ; **C3**:  $\frac{\gamma_k}{\eta_k} \leq \frac{\gamma_{k+1}}{\eta_{k+1}}$ . Then,

$$\frac{1}{\sqrt{N}} \| \mathbf{W}_k - \tilde{\mathbf{W}}_k \|_{\mathbb{E}} \leq \left[ \sum_{t=\bar{k}}^{k-1} P_{t+1,k}^2 \left( \gamma_t^2 \Sigma^{(1)} + \eta_t^2 \Sigma^{(2)} \right) \right]^{\frac{1}{2}}, \quad (27)$$

$$\begin{aligned} & \frac{1}{\sqrt{N}} \| \tilde{\mathbf{W}}_k - \mathbf{W}_k^* \|_{\mathbb{E}} \leq \text{dm}(\mathcal{W}) \cdot P_{\bar{k},k} \\ & + \frac{\nabla^* L}{\mu \rho_2} \sum_{t=\bar{k}}^{k-1} P_{t+1,k} \left( 1 + \frac{L^2 \eta_t}{\mu \rho_2 \gamma_t} \right) \left( \frac{\eta_t}{\gamma_t} - \frac{\eta_{t+1}}{\gamma_{t+1}} \right), \quad (28) \end{aligned}$$

$$\frac{1}{\sqrt{N}} \| \mathbf{W}_k^* - \mathbf{W}^* \| \leq \frac{\nabla^* L \eta_k}{\mu \rho_2 \gamma_k}. \quad (29)$$

where we have defined  $P_{t,k} \triangleq \Pi_{j=t}^{k-1} (1 - \mu \eta_j)$ ,  $k \geq t$ . (30)

*Proof.* See Appendix B.  $\square$

The term (27) captures the impact of the noise through the variance terms  $\Sigma^{(1)}$  and  $\Sigma^{(2)}$ . Eq. (28) is composed of two terms: the first  $(\text{dm}(\mathcal{W})P_{\bar{k},k})$  accounts for the initial error at time  $\bar{k}$ ; the second is a direct result of time-varying stepsizes (in fact, it is zero for constant ones); as highlighted previously, it represents the error accumulation due to tracking the changes of the  $G_k$ -minimizer  $\mathbf{W}_k^*$  over  $k$ . Eq. (29) shows that the minimizer  $\mathbf{W}_k^*$  of  $G_k$  approximates  $\mathbf{W}^*$  arbitrarily well when  $\eta_k/\gamma_k$  is small. We now specialize Theorem 1 to the case of constant stepsizes (Sec. IV.D), to gain insights on the design of decreasing stepsizes in Sec. IV.E.

#### D. Constant stepsizes

Let  $\eta_k = \eta > 0$ ,  $\gamma_k = \gamma > 0$ ,  $\forall k$ . For the sake of exposition, further assume  $\Sigma^{(2)} = 0$ , and consider a target timeframe  $K$  when the algorithm stops. To satisfy **C1-C2** of Theorem 1,

we need  $\eta(\mu+L) + \gamma \rho_N \leq 2$  and  $\frac{\eta}{\gamma} \leq \frac{\zeta \cdot \mu \rho_2}{\sqrt{N} \nabla^* L}$  with  $\bar{k} = 0$ . Then, at algorithm termination (27)-(29) specialize to

$$\frac{1}{\sqrt{N}} \| \mathbf{W}_K - \tilde{\mathbf{W}}_K \|_{\mathbb{E}} \leq \sqrt{\Sigma^{(1)}} \frac{\gamma}{\sqrt{\eta \mu}}, \quad (31)$$

$$\frac{1}{\sqrt{N}} \| \tilde{\mathbf{W}}_K - \mathbf{W}_K^* \|_{\mathbb{E}} \leq \text{dm}(\mathcal{W}) P_{0,K} \leq \text{dm}(\mathcal{W}) e^{-\mu \eta K}, \quad (32)$$

$$\frac{1}{\sqrt{N}} \| \mathbf{W}_K^* - \mathbf{W}^* \| \leq \frac{\nabla^* L \eta}{\mu \rho_2 \gamma}. \quad (33)$$

To make these errors small,  $\gamma/\sqrt{\eta}$ ,  $\eta/\gamma$  and  $e^{-\mu \eta K}$  need all be small, yielding a trade-off between  $\gamma$  and  $\eta$ . To make  $e^{-\mu \eta K} \rightarrow 0$  as  $K \rightarrow \infty$  we require  $\eta \propto K^{-(1-\epsilon)}$  for small  $\epsilon > 0$ . With such choice of  $\eta$ , the trade-off between (31) and (33) is optimized by making  $\gamma/\sqrt{\eta} \propto \eta/\gamma$ , yielding  $\gamma \propto K^{-3/4(1-\epsilon)}$ . Under this choice, the three error terms (31)-(33), hence the overall error (25), become of order  $\mathcal{O}(K^{-1/4(1-\epsilon)})$  for target  $K$  iterations. A similar convergence rate is shown in [21] under a different setup:<sup>8</sup> it assumes quantization, error-free communications, constant stepsizes and no projection. This analysis unveils some drawbacks of using constant stepsizes: 1) faster convergence is achieved with smaller  $\epsilon$  (approaching  $\mathcal{O}(K^{-1/4})$ ), at the cost of larger (32); 2) tuning of  $\eta$  and  $\gamma$  requires prior knowledge of the target timeframe  $K$ , as well as of  $\rho_2$ ,  $\rho_N$ ,  $\zeta$ ,  $\nabla^*$  to satisfy **C1-C2** of Theorem 1; 3) the step-size conditions needed to ensure these convergence properties may be excessively stringent to meet in practical scenarios. These limitations are overcome via decreasing stepsizes.

#### E. Decreasing stepsizes

The constant stepsize analysis suggests that  $\gamma_k \propto k^{-3/4}$  and  $\eta_k \propto k^{-1}$ . Accordingly, we choose  $\gamma_k = \gamma_0 (1 + k/\delta)^{-3/4}$  and  $\eta_k = \eta_0 (1 + k/\delta)^{-1}$  with initial stepsizes  $\gamma_0$ ,  $\eta_0$ , and delay factor  $\delta > 0$  preventing  $\eta_k, \gamma_k$  from decaying too quickly. Under this choice: 1)  $\gamma_k/\eta_k$  is non-decreasing in  $k$  (**C3** of Theorem 1); 2) since  $\eta_k, \gamma_k, \eta_k/\gamma_k \rightarrow 0$  for  $k \rightarrow \infty$ , there exists  $\bar{k} \geq 0$  such that **C1-C2** of Theorem 1 are satisfied  $\forall k \geq \bar{k}$ . The following result specializes Theorem 1 to this choice.

**Theorem 2.** Let  $\gamma_k = \gamma_0 (1 + k/\delta)^{-3/4}$ ,  $\eta_k = \eta_0 (1 + k/\delta)^{-1}$  with  $\delta \geq \frac{5}{4\mu\eta_0}$ . Then,  $\forall k \geq \bar{k}$ ,

$$\begin{aligned} & \frac{1}{\sqrt{N}} \| \mathbf{W}_k - \tilde{\mathbf{W}}_k \|_{\mathbb{E}} \leq \frac{\sqrt{5}e}{2\sqrt{\mu}} \left[ \frac{\gamma_0}{\sqrt{\eta_0}} \sqrt{\Sigma^{(1)}} \right. \\ & \left. + \sqrt{\eta_0 \Sigma^{(2)}} \left( 1 + \frac{k}{\delta} \right)^{-1/4} \right] \left( 1 + \frac{k}{\delta} \right)^{-1/4}, \quad (34) \end{aligned}$$

$$\begin{aligned} & \frac{1}{\sqrt{N}} \| \tilde{\mathbf{W}}_k - \mathbf{W}_k^* \|_{\mathbb{E}} \leq \text{dm}(\mathcal{W}) \left( 1 + \frac{k - \bar{k}}{\bar{k} + \delta} \right)^{-5/4} + \frac{\nabla^* L e \eta_0}{\mu \rho_2 4 \gamma_0} \\ & \times \left( 1 + \frac{L^2 \eta_0}{\mu \rho_2 \gamma_0} \left( 1 + \frac{k}{\delta} \right)^{-1/4} \right) \left( 1 + \frac{k}{\delta} \right)^{-1/4}, \quad (35) \end{aligned}$$

$$\frac{1}{\sqrt{N}} \| \mathbf{W}_k^* - \mathbf{W}^* \| \leq \frac{\nabla^* L \eta_0}{\mu \rho_2 \gamma_0} \left( 1 + \frac{k}{\delta} \right)^{-1/4}. \quad (36)$$

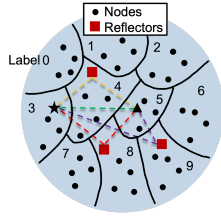
*Proof.* See Appendix C.  $\square$

Remarkably, this result holds true for any initial stepsizes  $\eta_0, \gamma_0 > 0$ , unlike the constant stepsize case which demands strict adherence to conditions **C1-C2**. This flexibility allows for numerical optimization of  $\eta_0$  and  $\gamma_0$  while maintaining the

<sup>8</sup>Note that  $\alpha, \epsilon, \delta, T$  used in [21, Theorem 1] map as  $\alpha \mapsto \eta/\gamma$ ,  $\epsilon \mapsto \gamma$ ,  $\delta \mapsto (1-\epsilon)/2$ ,  $T \mapsto K$  in our paper



Fig. 2: Example of *spatially dependent* deployment scenario with  $N = 40$  nodes. Each node holds data from only one class, indicated by the label indices '0' to '9' (4 nodes per class). For instance, node  $\star$  holds data from class '3'. With 3 reflectors, there are 4 signal paths, shown in the figure between a generic transmitter ( $\star$ ) and receiver ( $\blacktriangle$ ) pair.



convergence guarantees of Theorem 2, highlighting a trade-off in their selection. Tuning  $\gamma_0$  reflects a delicate balance between speeding up information propagation (favored by larger  $\gamma_0$ ) and minimizing error propagation (smaller  $\gamma_0$ ). As to the choice of  $\delta$ , as it diminishes, both  $\eta_k$  and  $\gamma_k$  decrease, reducing  $\kappa$ -the iteration index meeting the convergence conditions of Theorem 1. Thus, the regime  $k \geq \bar{\kappa}$  is attained more rapidly. At the same time, expressions like  $(1+k/\delta)^{-1/4}$  and  $(1+(k-\bar{\kappa})/(\bar{\kappa}+\delta))^{-5/4}$  decrease when  $\delta$  is reduced. We conclude that  $\delta = \frac{5}{4\mu\eta_0}$  minimizes (34)-(36), further motivating the use of decreasing vs constant ( $\delta \rightarrow \infty$ ) stepsizes (corroborated numerically in the supplemental document, see Fig. 5).

Combining these results into (26), it readily follows that

$$\mathbb{E} \left[ \frac{1}{N} \sum_i \|\mathbf{w}_{i,k} - \mathbf{w}^*\|^2 \right] = \mathcal{O}(1/\sqrt{k}). \quad (37)$$

To get some intuition behind this result, consider (21) with fixed consensus stepsize and no projection:

$$\mathbf{W}_{k+1} = (\mathbf{I} - \gamma \hat{\mathbf{L}}) \mathbf{W}_k - \eta_k \nabla f(\mathbf{W}_k) + \boldsymbol{\epsilon}_k^{(tot)}, \quad (38)$$

where  $\boldsymbol{\epsilon}_k^{(tot)} \triangleq \gamma \boldsymbol{\epsilon}_k^{(1)} - \eta_k \boldsymbol{\epsilon}_k^{(2)}$  is the overall noise. These updates resemble the DGD algorithm (1), where  $\mathbb{E}[\|\mathbf{W}_k^* - \mathbf{W}^*\|^2] = \mathcal{O}(1/k)$  with stepsize  $\eta_k \propto 1/k$ , provided that  $\text{var}(\boldsymbol{\epsilon}_k^{(tot)}) \propto k^{-2}$ . This condition holds when stochastic gradients are the sole noise source, since  $\|-\eta_k \boldsymbol{\epsilon}_k^{(2)}\|_{\mathbb{R}^d}^2 \propto \eta_k^2 \propto k^{-2}$ , but it fails in the presence of consensus error, which becomes dominant. To mitigate this additional noise source, a decreasing consensus stepsize  $\gamma_k \propto k^{-3/4}$  is required, at the expense of slower convergence ( $\mathcal{O}(1/\sqrt{k})$ ).

## V. NUMERICAL RESULTS

We solve a classification task on fashion-MNIST [22], a dataset of grayscale images of fashion items from 10 classes. **Network deployment:**  $N$  nodes ( $= 200$ , unless otherwise stated) are spread uniformly at random over a circular area of 2km radius. They communicate over a  $W_{\text{tot}}=5\text{MHz}$  bandwidth,  $f_c=3\text{GHz}$  carrier frequency, with  $P_{tx}=20\text{dBm}$  power ( $E = P_{tx}/W_{\text{tot}}$ ). The noise power spectral density at the receivers is  $N_0 = -173\text{dBm/Hz}$ . We use OFDM signaling with  $SC=512$  subcarriers and a cyclic prefix of length  $CP=133$ , accommodating propagation delays up to  $26.6\mu\text{s}$ . Each OFDM symbol has duration  $T_{\text{ofdm}}=(SC+CP)/W_{\text{tot}}=129\mu\text{s}$ .

**Channel model:** We generate spatially consistent channels by randomly placing 3 reflectors (see Fig. 2). The channel between transmitter  $j$  and receiver  $i$  in the  $m$ th subcarrier is

$$[\mathbf{h}_{i,j}]_m = \sum_{p=0}^3 \sqrt{\alpha_{i,j,p}} \phi_{i,j,p} e^{-j2\pi\tau_{i,j,p}} W_{\text{tot}} m / M,$$

where  $p=0$  is the LOS path and  $p \neq 0$  are the reflected paths;  $\tau_{i,j,p} = \frac{d_{i,j,p}}{c}$  is the path propagation delay,  $d_{i,j,p}$  is its distance traveled,  $c$  is the speed of light;  $\alpha_{i,j,p} = \left(\frac{c}{4\pi f_c d_{i,j,p}}\right)^2$  is the path gain, based on Friis' free space equation;  $\phi_{i,j,p}$  is the fading coefficient:  $|\phi_{i,j,p}|=1$  with uniform phase for the LOS path,  $\phi_{i,j,p} \sim \mathcal{CN}(0, 1)$  (Rayleigh fading) for reflected paths.

**Data deployment:** The global dataset is constituted of 1000 low-resolution images (100 from each class), distributed across the  $N$  nodes. To emulate data heterogeneity, each node has a local dataset with  $1000/N$  images *from a single class*,  $c_i \in \{0, \dots, 9\}$  for node  $i$ , so that  $N/10$  nodes have label (fashion item) '0',  $N/10$  have label '1', and so on. Cooperation is then necessary to solve the classification task, due to lack of examples of other classes at any single node. Each  $7 \times 7$  pixels image is converted into a 50-dimensional feature  $\mathbf{f} \in \mathbb{R}^{50}$  (including a fixed offset) and normalized to  $\|\mathbf{f}\|_2 = 1$ .

Furthermore, we consider two different spatial data distributions. In the *spatially-i.i.d.* case, the nodes' labels are assigned in an i.i.d. fashion to each node, irrespective of their location. In the *spatially-correlated* case, shown in Fig. 2, the circular region is divided into 10 subregions, each containing an equal number of nodes with the same label, so that the label of a certain node depends on its position in the network.

**Optimization problem:** We solve the task via regularized cross-entropy loss minimization, with loss function

$$\phi(c, \mathbf{f}; \mathbf{w}) = \frac{\mu}{2} \|\mathbf{w}\|_2^2 - \ln \left( \frac{\exp\{\mathbf{f}^\top \mathbf{w}^{(c)}\}}{\sum_{j=0}^9 \exp\{\mathbf{f}^\top \mathbf{w}^{(j)}\}} \right)$$

for feature  $\mathbf{f}$  with label  $c$ , where:  $\mathbf{w}^\top = [\mathbf{w}^{(1)\top}, \dots, \mathbf{w}^{(9)\top}] \in \mathbb{R}^d$  is a  $d=450$ -dimensional parameter vector, with  $\mathbf{w}^{(c)} \in \mathbb{R}^{50}$ ,  $\mathbf{w}^{(0)} = \mathbf{0}$ ,  $\mu = 0.001 > 0$ . Hence,  $f_i(\mathbf{w}) = \frac{1}{|\mathcal{D}_i|} \sum_{\mathbf{f} \in \mathcal{D}_i} \phi(c_i, \mathbf{f}; \mathbf{w})$ . All  $f_i(\mathbf{w})$  and the global function  $F(\mathbf{w})$  are  $\mu$ -strongly-convex and  $L = \mu + 2$ -smooth.  $\mathcal{W}$  is the  $d$ -dimensional sphere centered at  $\mathbf{0}$  with radius  $r = \frac{1}{\mu} \|\nabla F(\mathbf{0})\|$  (Example 1).

**Computational model:** Each gradient computation  $\nabla \phi(\cdot)$  on a single datapoint takes  $T_{\text{gr}} = 30\mu\text{s}$ .<sup>9</sup> Hence, computing the gradient over a minibatch  $\mathcal{B}_i \subseteq \mathcal{D}_i$  takes  $|\mathcal{B}_i| T_{\text{gr}}$ . Since gradient computations are done in parallel with communications, we set the minibatch size as  $|\mathcal{B}_i| = \min\{\lfloor T/T_{\text{gr}} \rfloor, |\mathcal{D}_i|\}$ , consistent with the frame duration  $T$  specific to each algorithm.

### A. Comparison of variants of NCOTA-DGD

We compare different configurations of NCOTA-DGD:

- **Baseline** uses the CP0 codebook of Example 1 with  $M=2d+1=901$  codewords, requiring two OFDM symbols ( $Q=1024$ ), and yielding a frame of duration  $T=2T_{\text{ofdm}}=258\mu\text{s}$ . It follows Algorithm 1 with parameters  $\eta_0 = \frac{2}{\mu+L}$ ,  $\gamma_0 = \frac{0.05}{\rho_2}$  and  $\delta = \frac{5}{4\mu\eta_0}$ , in line with Theorem 2 and as motivated in the discussion following Theorem 2. The transmission probability  $p_{\text{tx}}$  is set as in Lemma 1, with  $\vartheta=1$  and  $\zeta \approx \sqrt{M/Q}$ . This choice of parameters is corroborated by numerical evaluations in the supplemental document (Fig. 5).
- **2xOFDM** and **4xOFDM** are the same as *Baseline*, but they use  $\times 2$  and  $\times 4$  as many OFDM symbols, yielding  $Q=2048$  ( $T=516\mu\text{s}$ ) and  $Q=4096$  ( $T=1032\mu\text{s}$ ), respectively. From Lemma 1, larger  $Q$  yields smaller noise in the consensus estimation, at the cost of longer frame duration  $T$ .
- **CP** is the same as *Baseline*, but it employs the conventional cross-polytope codebook of [39] with  $\phi = 1 - \frac{1}{\sqrt{dr}} \|\mathbf{w}_i\|_1$ .
- **No random shifts** is the same as *Baseline*, but it does not apply the random phase and coordinated circular subcarrier shifts on the transmitted signal, described in Sec. III.B.

All variants are initialized as  $\mathbf{w}_i = \mathbf{0}, \forall i$ . We evaluate them on four different scenarios as described in the caption of Fig. 3, differing in the data deployments (spatially-i.i.d. or correlated) and channel fading properties: i.i.d., in which the channel

<sup>9</sup>Estimated based on a 2.4 GHz 8-Core Intel Core i9 processor.



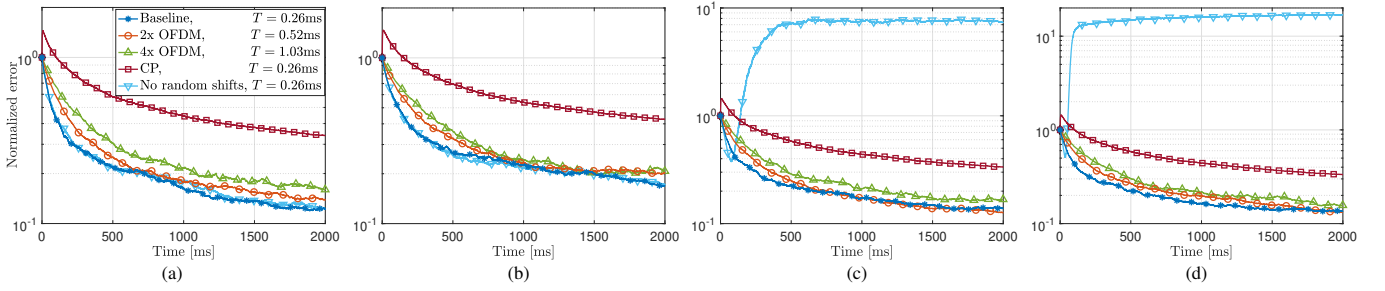


Fig. 3: Normalized error vs time, for different configurations of NCOTA-DGD and four different scenarios. The common legend is shown in the left figure, and shows the frame duration of each configuration. (a) Spatially-i.i.d. labels and i.i.d. channels; (b) Spatially-correlated labels and i.i.d. channels; (c) Spatially-i.i.d. labels and block-fading channels (2ms coherence time); (d) Spatially-i.i.d. labels and static channels.

fading is i.i.d. over frames; block-fading, in which they vary every 2ms (channels with a 2ms coherence time); and static, in which they remain fixed over the entire simulated interval.

In Fig. 3, we plot the *normalized error*,  $\frac{\hat{\mathbb{E}}[\sum_i \|\mathbf{w}_i - \mathbf{w}^*\|^2]}{N \|\mathbf{w}^*\|^2}$ , versus the execution time ( $kT$  after  $k$  iterations). Here,  $\hat{\mathbb{E}}$  denotes a sample average across 20 algorithm trajectories generated through independent realizations of network deployment, channels, AWGN noise, and randomness used by the algorithm (transmission decisions, phase and circular subcarrier shifts, minibatch gradient selections). We notice that *Baseline* consistently performs the best across all different scenarios. It has shorter frame duration but higher variance of the disagreement signal estimation (Lemma 1) than *2xOFDM* and *4xOFDM*. This demonstrates that it is preferable to perform more frequent, albeit more noisy, iterations of DGD. The CP0 codebook of *Baseline* has lower variance of the disagreement signal estimation than *CP*, yielding better performance.<sup>10</sup> *No random shifts* diverges when the channels are not i.i.d. (Figs. 3.c-d), due to a bias term in the disagreement signal estimation (see (12)), which accumulates over time. In contrast, all other schemes employing the random phase and circular subcarrier shifts developed in Sec. III.B are not affected by different channel fading properties. Fig. 3.b depicts a slight degradation in performance for all schemes in the spatially-correlated label scenario. To explain this behavior, consider the receiving node labeled as  $\blacktriangle$  in Fig. 2, carrying label '5': it receives strong signals from the nearby nodes carrying the same label '5' (less informative to  $\blacktriangle$ ), but weaker signals from the nodes with label '0' (more informative to  $\blacktriangle$ ). This results in slower propagation of information across the network.

### B. Comparison with state-of-the-art (SoA) schemes

We now compare NCOTA-DGD with adaptation of SoA works to the setting of this paper. We use the *Baseline* configuration described in Sec. V.A, due to its superior performance observed in Fig. 3. We also evaluate the following SoA schemes.

- *QDGD-LPQ/VQ*, adaptations of [21], which investigates the design and convergence analysis of Quantized-DGD under fixed learning and consensus stepsizes. Yet, it assumes error-free communications, hence is not tailored to wireless systems affected by fading and interference. To adapt [21] to our setting, nodes transmit over orthogonal channels via OFDMA, i.e., multiple nodes may transmit simultaneously on the same OFDM symbol, across orthogonal subcarriers. Node  $i$  quantizes  $\mathbf{w}_i$  using  $B$  bits, and broadcasts the payload over the wireless channel on the assigned subcarriers  $\mathcal{S}_i$ . Upon

receiving the signal broadcast by node  $j$ , node  $i$  decodes the payload correctly (denoted by the success indicator  $\chi_{i,j}=1$ ) if and only if  $B < \sum_{s \in \mathcal{S}_j} \log_2(1 + \frac{E}{N_0} \frac{SC}{|\mathcal{S}_j|} |\mathbf{h}_{i,j}|_s|^2)$ , where  $\mathcal{S}_j$  are the subcarriers allocated to node  $j$ . Otherwise, an outage occurs ( $\chi_{i,j}=0$ ). Let  $N_{rx,i}$  be the number of packets successfully received, and  $\hat{\mathbf{w}}_j$  the reconstruction of  $\mathbf{w}_j$  induced by the quantization operator. Node  $i$  then follows the updates (9), with  $\hat{\mathbf{d}}_i = \frac{1}{N_{rx,i}} \sum_j \chi_{i,j} (\hat{\mathbf{w}}_j - \mathbf{w}_i)$ .

We consider two quantization schemes. The low precision quantizer (LPQ, see [21, Example 2]) normalizes  $\mathbf{w}_i$  by  $\|\mathbf{w}_i\|_\infty$ , and then quantizes each component of  $\mathbf{w}_i / \|\mathbf{w}_i\|_\infty \in [-1, 1]^d$  with  $b$  bits using dithered quantization. The overall payload is  $B=64+b \cdot d$  bits, including the magnitude  $\|\mathbf{w}_i\|_\infty$  encoded with machine precision (64 bits). The cross-polytope vector quantization (VQ) technique [39] with REP repetitions to reduce the variance of the quantization noise. Since the cross-polytope codebook contains  $2d$  codewords, the overall payload with REP repetitions is  $B=\text{REP} \lceil \log_2(2d) \rceil$ . The free parameters (number of subcarriers  $SC_n$  per node, bits for LPQ, repetitions for VQ) are optimized numerically for best performance. *The constant consensus and learning stepsizes are also optimized numerically, hence may not satisfy the stringent conditions of [21]*. Since one OFDM symbol fits  $\frac{SC}{SC_n}$  transmissions, the frame duration is  $T=N \cdot \frac{SC_n}{SC} \cdot T_{\text{ofdm}}$ .

- *AirComp-D2D*, inspired by [18], leverages over-the-air computation (AirComp) to efficiently solve DGD over device-to-device mesh networks. It organizes the network into non-interfering, star-based sub-networks via graph coloring, scheduling multiple such sub-networks simultaneously to enhance spectral efficiency. Each sub-network operates in paired slots: in the first, the central node receives coherently aggregated models from neighbors via AirComp with channel inversion; in the second, it broadcasts its own model to its neighbors. This process continues until all D2D links have been activated. We generate the mesh network based on a maximum distance criterium, i.e. nodes  $i, j$  are connected if and only if they are less than  $\text{dist}_{\max}$  apart. We use the Metropolis-Hastings rule to design the mixing weights  $\omega_{i,j}$  [48]. While [18] assumes Rayleigh flat-fading channels with no interference between non-neighboring devices, our adaptation extends to frequency-selective channels and accounts for interference. Note that *AirComp-D2D* requires CSI for power control, relies on *instantaneous* channel reciprocity for channel inversion, and requires centralized knowledge of the graph topology for graph coloring. In contrast, NCOTA-DGD does not require any such knowledge, and relies only on *average* (vs *instantaneous*) channel gain reciprocity,  $\Lambda_{i,j}=\Lambda_{j,i}$ . The free parameters ( $\text{dist}_{\max}$ , stepsizes) are optimized numerically for

<sup>10</sup>Analysis of this behavior is left for future work; it requires a tighter bound than Lemma 1 (valid under any codebook), by exploiting properties of CP0.

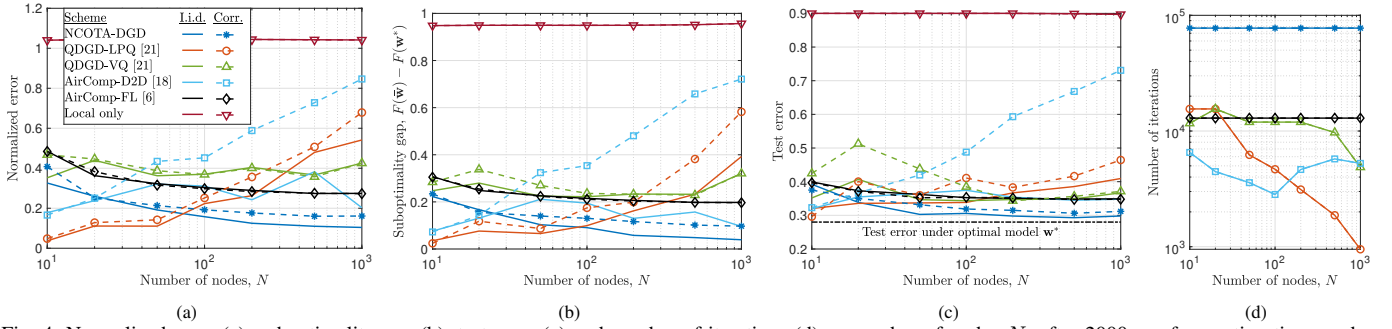


Fig. 4: Normalized error (a), suboptimality gap (b), test error (c) and number of iterations (d) vs number of nodes  $N$ , after 2000ms of execution time, under spatially-i.i.d. (solid lines) and -correlated (dashed lines with markers) label scenarios, with i.i.d. channels over frames. Common legend shown in figure (a).

best performance. We refer to [18] for further details.

- *AirComp-FL*, based on [6], solves  $\{P\}$  via federated learning (FL) across a star topology, with one node acting as the parameter server (PS, the star center). The process unfolds in three stages: first, the PS sends the current model to the  $N - 1$  edge devices; then, each device updates this model via *local gradient descent*; finally, all devices simultaneously send their updates to the PS using AirComp with channel inversion, enabling the PS to update the model for the next round. Like [18], this approach relies on instantaneous channel reciprocity and CSI, obtained by broadcasting an OFDM in the downlink.
- *Local only*: Nodes optimize independently using their datasets, without inter-node communication. This scheme illustrates the need for communication to solve the ML task: it results in a 90% test error, as shown in Fig. 4.c.

In Fig. 4, we compare these schemes versus the number of nodes  $N$ , after  $T_{sim}=2000$ ms of execution time. Note that the number of iterations completed by a certain scheme is  $\sim T_{sim}/T$ , function of its frame duration  $T$ , shown in Fig. 4.d, for each scheme. In addition to the normalized error (a), we also evaluate the *suboptimality gap* of the average model  $\bar{\mathbf{w}} = \frac{1}{N} \sum_i \mathbf{w}_i$ ,  $F(\bar{\mathbf{w}}) - F(\mathbf{w}^*)$  (b) and the *test error*  $\text{TEST}(\bar{\mathbf{w}})$ , computed on a test set of 1000 examples (100 for each class). For a parameter vector  $\mathbf{w}^T = [\mathbf{w}^{(1)T}, \dots, \mathbf{w}^{(9)T}] \in \mathbb{R}^d$  and  $\mathbf{w}^{(0)} = \mathbf{0}$ , we predict the class associated to feature vector  $\mathbf{d}$  as  $\arg \max_c \bar{\mathbf{w}}^{(c)T} \mathbf{f}$ . The results are further averaged over 20 algorithm trajectories generated through independent realizations of network deployment, channels, AWGN noise, and randomness used by each algorithm.

Overall, smaller normalized error typically translates to smaller suboptimality gap and test error. NCOTA-DGD performs the best when  $N \geq 100$ , under both spatially-i.i.d. and correlated label scenarios. In fact, it executes the most iterations (Fig. 4.d) within the execution time  $T_{sim}$ , revealing its scalability to dense network deployments; in contrast, all other schemes, with the exception of *AirComp-FL* and *AirComp-D2D*, execute less iterations as  $N$  increases, due to the increased scheduling overhead. For smaller networks ( $N < 100$ ), *QDGD-LPQ* performs the best: in this regime, it schedules all devices within a small frame duration, yet it has better noise control through the use of digital transmissions, and avoids interference via OFDMA scheduling.

*AirComp-D2D* performs well across  $N$  in the spatially-i.i.d. label scenario (between 3k and 6k iterations across all  $N$ , see Fig. 4.d), thanks to its efficient scheduling and the use of AirComp allowing simultaneous transmissions [18]. Yet, it performs poorly in the spatially-correlated label sce-

nario, due to the slower propagation of information across the network, noted in the evaluations of Sec. V.A. With *AirComp-D2D*, information propagation is further hampered by the D2D connectivity structure, so that it takes several iterations for the information generated by the nodes at the edge to propagate through the mesh network to the rest of the network. In contrast, NCOTA-DGD does not rely on a predetermined D2D mesh network: it exploits the channel propagation conditions in the consensus phase, resulting in a much smaller performance degradation.

*AirComp-FL* also exhibits scalability with respect to  $N$  through AirComp. Yet, its effectiveness is limited by channel estimation errors and the star topology's vulnerability to pathloss, especially affecting edge devices. This results in a communication bottleneck: uplink transmissions must accommodate the worst channel conditions to satisfy power constraints during channel inversion; in the downlink, transmission rates are reduced to guarantee reception by the edge devices. Conversely, NCOTA-DGD is topology-agnostic and leverages actual channel conditions in the consensus phase.

## VI. CONCLUSIONS

This paper presents a novel DGD algorithm tailored to wireless systems, addressing the challenges posed by noise, fading, and bandwidth constraints without requiring inter-agent coordination, topology, or channel state information. Our approach, centered around a Non-Coherent Over-The-Air (NCOTA) consensus mechanism, leverages a natural energy superposition property of wireless channels, allowing simultaneous, uncoordinated transmissions. This novel method achieves efficient consensus estimation without explicit mixing weights, exploiting pathloss and adapting to a variety of fading and channel conditions. We prove that the error of NCOTA-DGD vanishes with rate  $\mathcal{O}(k^{-1/2})$  after  $k$  iterations, using suitably tuned consensus and learning stepsizes. Our results indicate a promising direction for decentralized optimization in wireless environments, showcasing faster convergence and operational efficiency, especially in densely populated networks.

*Acknowledgments*: Special thanks to Prof. Gesualdo Scutari for valuable discussions during manuscript preparation.

### APPENDIX A: BOUND ON THE SGD VARIANCE

**Lemma 2.** Assume  $|D_i| = D \geq 2$ ,  $\forall i$  and minibatch gradients with minibatch size  $|\mathcal{B}_{i,k}| = B \in \{1, \dots, D\}$ ,  $\forall i, k$ . Assume that:  $\{1\}$  the loss function  $\phi(\boldsymbol{\xi}; \mathbf{w})$  is  $\mu$  strongly-convex and  $L$  smooth with respect to  $\mathbf{w}$  (implying Assumption 2);  $\{2\}$   $\|\nabla \phi(\boldsymbol{\xi}; \mathbf{w}^*)\| \leq \nabla^*$ ,  $\forall \boldsymbol{\xi} \in D_i, \forall i$  (implying Def. 2). Then,

$$\frac{1}{N} \mathbb{E}[\|\boldsymbol{\epsilon}_k^{(2)}\|^2 | \mathcal{F}_k] \leq \frac{D-B}{B(D-1)} (\nabla^* + L \cdot \text{dm}(\mathcal{W}))^2 \triangleq \Sigma^{(2)}.$$

*Proof.* It directly follows from [49, Prop. 1], along with  $\|\nabla\phi(\boldsymbol{\xi}; \mathbf{w})\| \leq \|\nabla\phi(\boldsymbol{\xi}; \mathbf{w}^*)\| + \|\nabla\phi(\boldsymbol{\xi}; \mathbf{w}) - \nabla\phi(\boldsymbol{\xi}; \mathbf{w}^*)\| \leq \nabla^* + L\|\mathbf{w} - \mathbf{w}^*\| \leq \nabla^* + L \cdot \text{dm}(\mathcal{W})$ .  $\square$

## APPENDIX B: PROOF OF THEOREM 1

We prove (27)-(29) in appendices B.I-B.III, using the auxiliary lemmas in B.IV. We denote the set of semidefinite-positive  $n \times n$  matrices with eigenvalues in the interval  $[\mu, L]$  as  $\mathcal{S}_{\mu, L}^n$ . We start with two important properties.

**P1:** For any twice-differentiable function  $f: \mathbb{R}^n \mapsto \mathbb{R}$ ,  $\mu$ -strongly convex and  $L$ -smooth, we can express  $\nabla f(\mathbf{y})$  as the line integral of the Hessian matrix  $\nabla^2 f$  between  $\mathbf{x}$  and  $\mathbf{y}$ :

$$\begin{aligned} \nabla f(\mathbf{y}) &= \nabla f(\mathbf{x}) + \int_0^1 \nabla^2 f(\mathbf{x} + t(\mathbf{y} - \mathbf{x})) dt (\mathbf{y} - \mathbf{x}), \\ &= \nabla f(\mathbf{x}) + \mathbf{A}(\mathbf{y} - \mathbf{x}), \end{aligned} \quad (39)$$

where  $\mathbf{A}$  (function of  $\mathbf{x}$ ,  $\mathbf{y}$ ) is the *mean Hessian* matrix between points  $\mathbf{x}$  and  $\mathbf{y}$ . Since  $f$  is  $\mu$ -strongly convex and  $L$ -smooth, it follows that  $\nabla^2 f \in \mathcal{S}_{\mu, L}^n$ , hence  $\mathbf{A} \in \mathcal{S}_{\mu, L}^n$ .

**P2:** For any function  $h: \mathbb{R}^n \mapsto \mathbb{R}$ ,  $\mu_h$ -strongly convex and  $L_h$ -smooth ( $L_h \geq \mu_h$ ), any  $\mathbf{x}, \mathbf{y} \in \mathbb{R}^n$ , and stepsize  $\eta \in [0, \frac{2}{\mu_h + L_h}]$ ,

$$\|(\mathbf{x} - \mathbf{y}) - \eta(\nabla h(\mathbf{x}) - \nabla h(\mathbf{y}))\| \leq (1 - \eta\mu_h)\|\mathbf{x} - \mathbf{y}\|. \quad (40)$$

To prove it, use (39) to express  $\nabla h(\mathbf{y}) = \nabla h(\mathbf{x}) + \mathbf{A}(\mathbf{y} - \mathbf{x})$  and  $\|(\mathbf{x} - \mathbf{y}) - \eta(\nabla h(\mathbf{x}) - \nabla h(\mathbf{y}))\|^2 = \|(\mathbf{I} - \eta\mathbf{A})(\mathbf{x} - \mathbf{y})\|^2$ , where  $\mathbf{A} \in \mathcal{S}_{\mu_h, L_h}^n$ . Since  $\mathbf{A} \in \mathcal{S}_{\mu_h, L_h}^n$ , we further bound

$$\|(\mathbf{I} - \eta\mathbf{A})(\mathbf{x} - \mathbf{y})\|^2 \leq \max_{\rho \in [\mu_h, L_h]} (1 - \eta\rho)^2 \|\mathbf{x} - \mathbf{y}\|^2.$$

It is straightforward to show that the right-hand-side is maximized by  $\rho = \mu_h$  under the stepsize assumption, yielding (40).

### Appendix B.I: Proof of (27)

Using the non-expansive property of projections (see, for instance, [50]), we can bound  $\|\mathbf{W}_{k+1} - \tilde{\mathbf{W}}_{k+1}\|^2$

$$\leq \|\mathbf{W}_k - \tilde{\mathbf{W}}_k - \eta_k(\nabla G_k(\mathbf{W}_k) - \nabla G_k(\tilde{\mathbf{W}}_k)) + \gamma_k \boldsymbol{\epsilon}_k^{(1)} - \eta_k \boldsymbol{\epsilon}_k^{(2)}\|^2.$$

Taking the expectation conditional on  $\mathcal{F}_k$  and using the independence of  $\boldsymbol{\epsilon}_k^{(1)}$  and  $\boldsymbol{\epsilon}_k^{(2)}$ , it follows  $\mathbb{E}[\|\mathbf{W}_{k+1} - \tilde{\mathbf{W}}_{k+1}\|^2 | \mathcal{F}_k]$

$$\leq \|(\mathbf{W}_k - \tilde{\mathbf{W}}_k) - \eta_k(\nabla G_k(\mathbf{W}_k) - \nabla G_k(\tilde{\mathbf{W}}_k))\|^2 \quad (41)$$

$$+ \gamma_k^2 N \Sigma^{(1)} + \eta_k^2 N \Sigma^{(2)}. \quad (42)$$

Note that Assumption 2 implies that  $G_k$  is  $\mu$ -strongly convex and  $L_{G,k} \triangleq L + \frac{\gamma_k}{\eta_k} \rho_N$ -smooth. Then, using (40), we find that (41)  $\leq (1 - \mu\eta_k)^2 \|\mathbf{W}_k - \tilde{\mathbf{W}}_k\|^2$ , as long as  $\eta_k \leq 2/(\mu + L_{G,k})$  (C1 of Theorem 1). Using this bound and computing the unconditional expectation, it follows  $\|\mathbf{W}_{k+1} - \tilde{\mathbf{W}}_{k+1}\|_{\mathbb{E}}^2$

$$\leq (1 - \mu\eta_k)^2 \|\mathbf{W}_k - \tilde{\mathbf{W}}_k\|_{\mathbb{E}}^2 + \gamma_k^2 N \Sigma^{(1)} + \eta_k^2 N \Sigma^{(2)}.$$

The result follows by induction and noting that  $\mathbf{W}_{\bar{k}} = \tilde{\mathbf{W}}_{\bar{k}}$ .

### Appendix B.II: Proof of (29)

Let  $\hat{\mathbf{W}}_k \triangleq \arg \min_{\mathbf{W} \in \mathbb{R}^{Nd}} G_k(\mathbf{W})$  be the *unconstrained* minimizer of  $G_k$ ;<sup>11</sup> this is in contrast to  $\mathbf{W}_k^*$ , which minimizes it over  $\mathcal{W}^N$ . In the last part of the proof, we will show that, when  $\frac{\eta_k}{\gamma_k} \leq \frac{\zeta \cdot \mu \rho_2}{\sqrt{N} \nabla^* L}$  (C2 of Theorem 1),  $\mathbf{W}_k^*$  and  $\hat{\mathbf{W}}_k$  coincide.

<sup>11</sup>Here, we assume that all  $f_i$ 's are defined on  $\mathbb{R}^d$ , and the extended functions are  $L$ -smooth and  $\mu$ -strongly convex on  $\mathbb{R}^d$

Since  $G_k$  is strongly-convex and smooth on  $\mathbb{R}^{Nd}$ ,  $\hat{\mathbf{W}}_k$  is the unique solution of  $\nabla G_k(\hat{\mathbf{W}}_k) = \mathbf{0}$  in  $\mathbb{R}^{Nd}$ . We now bound the distance of  $\hat{\mathbf{W}}_k$  from  $\mathbf{W}^*$ . From (39) with  $\mathbf{x} = \mathbf{W}^*$ ,  $\mathbf{y} = \hat{\mathbf{W}}_k$ , there exists  $\mathbf{A} \in \mathcal{S}_{\mu, L}^{Nd}$  such that

$$\nabla f(\hat{\mathbf{W}}_k) = \nabla f(\mathbf{W}^*) + \mathbf{A}(\hat{\mathbf{W}}_k - \mathbf{W}^*).$$

It follows that  $\mathbf{0} = \nabla G_k(\hat{\mathbf{W}}_k) - \frac{\gamma_k}{\eta_k} \hat{\mathbf{L}} \mathbf{W}^* = \nabla f(\hat{\mathbf{W}}_k) + \frac{\gamma_k}{\eta_k} \hat{\mathbf{L}}(\hat{\mathbf{W}}_k - \mathbf{W}^*) = \nabla f(\mathbf{W}^*) + \mathbf{B}(\hat{\mathbf{W}}_k - \mathbf{W}^*)$ , where we used  $\hat{\mathbf{L}} \mathbf{W}^* = (\mathbf{L} \otimes \mathbf{I}_d) \cdot (\mathbf{1}_N \otimes \mathbf{w}^*) = (\mathbf{L} \cdot \mathbf{1}_N) \otimes \mathbf{w}^* = \mathbf{0}$ , and defined  $\mathbf{B} \triangleq \mathbf{A} + \frac{\gamma_k}{\eta_k} \hat{\mathbf{L}} \geq \mu \mathbf{I}$ . Solving with respect to  $\hat{\mathbf{W}}_k - \mathbf{W}^*$  and computing the norm of both sides, we find

$$\|\hat{\mathbf{W}}_k - \mathbf{W}^*\| = \|\mathbf{B}^{-1} \nabla f(\mathbf{W}^*)\|. \quad (43)$$

Note that  $\nabla f(\mathbf{W}^*) \perp (\mathbf{1}_N \otimes \mathbf{I}_d)$  (in fact,  $\sum_i \nabla f_i(\mathbf{w}^*) = \mathbf{0}$  from the optimality condition on  $\mathbf{w}^*$ , since  $\mathbf{w}^* \in \text{int}(\mathcal{W})$ ). Hence, we bound (43) via Lemma 3 in B.IV with  $U = \frac{\gamma_k}{\eta_k}$  as

$$\|\hat{\mathbf{W}}_k - \mathbf{W}^*\| \leq \frac{L}{\mu \rho_2} \frac{\eta_k}{\gamma_k} \|\nabla f(\mathbf{W}^*)\| \leq \frac{\sqrt{N} \nabla^* L \eta_k}{\mu \rho_2 \gamma_k}, \quad (44)$$

where in the last step we used  $\|\nabla f(\mathbf{W}^*)\| \leq \sqrt{\sum_i \|\nabla f_i(\mathbf{w}^*)\|^2} \leq \sqrt{N} \nabla^*$  from Definition 2.

Next, we show that  $\hat{\mathbf{W}}_k \in \mathcal{W}^N$ , hence it coincides with the solution of the constrained problem ( $\hat{\mathbf{W}}_k = \mathbf{W}_k^*$ ). Since  $\mathbf{w}^*$  is at distance  $\zeta$  from the boundary of  $\mathcal{W}$  (Assumption 3), it suffices to show that  $\|\hat{\mathbf{w}}_{i,k} - \mathbf{w}^*\| \leq \zeta$ ,  $\forall i$  (i.e.,  $\mathbf{w}^*$  is closer to  $\hat{\mathbf{w}}_{i,k}$  than to the boundary of  $\mathcal{W}$ ). Indeed,  $\|\hat{\mathbf{w}}_{i,k} - \mathbf{w}^*\| \leq \|\hat{\mathbf{W}}_k - \mathbf{W}^*\| \leq \frac{\sqrt{N} \nabla^* L \eta_k}{\mu \rho_2 \gamma_k}$ , hence, when  $\frac{\eta_k}{\gamma_k} \leq \frac{\zeta \cdot \mu \rho_2}{\sqrt{N} \nabla^* L}$  (C2 of Theorem 1), it follows that  $\hat{\mathbf{W}}_k = \mathbf{W}_k^*$ ,

$$\nabla G_k(\mathbf{W}_k^*) = \mathbf{0}, \quad (45)$$

and (29) readily follows from (44).

### Appendix B.III: Proof of (28)

Using the triangle inequality, we bound

$$\|\tilde{\mathbf{W}}_{k+1} - \mathbf{W}_{k+1}^*\| \leq \|\tilde{\mathbf{W}}_{k+1} - \mathbf{W}_k^*\| + \|\mathbf{W}_{k+1}^* - \mathbf{W}_k^*\|. \quad (46)$$

Using the fixed point optimality condition  $\mathbf{W}_k^* = \Pi^N[\mathbf{W}_k^* - \eta \nabla G_k(\mathbf{W}_k^*)]$ ,  $\forall \eta \geq 0$  and the non-expansive property of projections [50], we bound the first term of (46) as  $\|\tilde{\mathbf{W}}_{k+1} - \mathbf{W}_k^*\|$

$$\begin{aligned} &= \|\Pi^N[\tilde{\mathbf{W}}_k - \eta_k \nabla G_k(\tilde{\mathbf{W}}_k)] - \Pi^N[\mathbf{W}_k^* - \eta_k \nabla G_k(\mathbf{W}_k^*)]\| \\ &\leq \|\tilde{\mathbf{W}}_k - \mathbf{W}_k^* - \eta_k(\nabla G_k(\tilde{\mathbf{W}}_k) - \nabla G_k(\mathbf{W}_k^*))\| \\ &\leq (1 - \mu\eta_k) \|\tilde{\mathbf{W}}_k - \mathbf{W}_k^*\|, \end{aligned} \quad (47)$$

where in the last step we used (40) since  $G_k$  is  $\mu$ -strongly convex and  $L_{G,k} \triangleq L + \frac{\gamma_k}{\eta_k} \rho_N$ -smooth, provided that  $\eta_k \leq 2/(\mu + L_{G,k})$  (C1 of Theorem 1). We now bound  $\|\mathbf{W}_{k+1}^* - \mathbf{W}_k^*\|$ . First, note that, for  $t \geq \bar{k}$ ,  $\mathbf{W}_t^*$  satisfies the optimality condition  $\nabla G_t(\mathbf{W}_t^*) = \mathbf{0}$  (see (45)). It then follows that

$$\mathbf{0} = \nabla G_{k+1}(\mathbf{W}_{k+1}^*) = \nabla f(\mathbf{W}_{k+1}^*) + \frac{\gamma_{k+1}}{\eta_{k+1}} \hat{\mathbf{L}} \mathbf{W}_{k+1}^*, \quad (48)$$

$$\mathbf{0} = \nabla G_k(\mathbf{W}_k^*) = \nabla f(\mathbf{W}_k^*) + \frac{\gamma_k}{\eta_k} \hat{\mathbf{L}} \mathbf{W}_k^*. \quad (49)$$

Furthermore, from (39) with  $\mathbf{x} = \mathbf{W}_k^*$  and  $\mathbf{y} = \mathbf{W}_{k+1}^*$ , there exists  $\mathbf{A} \in \mathcal{S}_{\mu, L}^{Nd}$  such that  $\nabla f(\mathbf{W}_{k+1}^*) = \nabla f(\mathbf{W}_k^*) + \mathbf{A}(\mathbf{W}_{k+1}^* - \mathbf{W}_k^*)$ . We use this expression in (48), subtract



(49), reorganize and solve. These steps yield

$$\mathbf{W}_{k+1}^* - \mathbf{W}_k^* = -\left(\frac{\gamma_{k+1}}{\eta_{k+1}} - \frac{\gamma_k}{\eta_k}\right) \mathbf{B}^{-1} \hat{\mathbf{L}} \mathbf{W}_{k+1}^*,$$

where  $\mathbf{B} \triangleq \mathbf{A} + \frac{\gamma_k}{\eta_k} \hat{\mathbf{L}}$ . Therefore,

$$\|\mathbf{W}_{k+1}^* - \mathbf{W}_k^*\| \leq \left(\frac{\gamma_{k+1}}{\eta_{k+1}} - \frac{\gamma_k}{\eta_k}\right) \|\mathbf{B}^{-1} \hat{\mathbf{L}} \mathbf{W}_{k+1}^*\|. \quad (50)$$

Noting that  $\hat{\mathbf{L}} \mathbf{W}_{k+1}^* \perp (\mathbf{1}_N \otimes \mathbf{I}_d)$  (since  $\mathbf{1}^\top \mathbf{L} = \mathbf{0}^\top$ ), we use Lemma 3 in B.IV with  $U = \frac{\gamma_k}{\eta_k}$  to bound

$$\|\mathbf{W}_{k+1}^* - \mathbf{W}_k^*\| \leq \frac{L}{\mu \rho_2} \left(\frac{\gamma_{k+1}}{\eta_{k+1}} - \frac{\gamma_k}{\eta_k}\right) \frac{\eta_k}{\gamma_k} \|\hat{\mathbf{L}} \mathbf{W}_{k+1}^*\|.$$

Finally, we bound  $\|\hat{\mathbf{L}} \mathbf{W}_{k+1}^*\|$  via Lemma 4 in Appendix B.IV:

$$\|\mathbf{W}_{k+1}^* - \mathbf{W}_k^*\| \leq \left(\frac{\eta_k}{\gamma_k} - \frac{\eta_{k+1}}{\gamma_{k+1}}\right) \frac{\sqrt{N} \nabla^* L}{\mu \rho_2} \left(1 + \frac{L^2}{\mu \rho_2} \frac{\eta_k}{\gamma_k}\right).$$

Eq. (28) follows by combining this result with (47) into (46), and solving via induction with  $\|\tilde{\mathbf{W}}_{\bar{k}} - \mathbf{W}_{\bar{k}}^*\| \leq \sqrt{N} \text{dm}(\mathcal{W})$ .

*Appendix B.IV: Auxiliary lemmas*

**Lemma 3.** Let  $\mathbf{B} = \mathbf{A} + U \hat{\mathbf{L}}$ , where  $U > 0$ ,  $\mathbf{A} \in \mathcal{S}_{\mu, L}^{N, d}$ . Then,

$$\|\mathbf{B}^{-1} \mathbf{v}\| \leq \frac{1}{U} \cdot \frac{L}{\mu \rho_2} \|\mathbf{v}\|, \quad \forall \mathbf{v} \perp (\mathbf{1}_N \otimes \mathbf{I}_d).$$

*Proof.* Using  $\mathbf{A} \succeq \mu \mathbf{I}$ , we start with bounding

$$\|\mathbf{B}^{-1} \mathbf{v}\| = \|\mathbf{A}^{-1} \mathbf{A} \mathbf{B}^{-1} \mathbf{v}\| \leq \frac{1}{\mu} \|\mathbf{A} \mathbf{B}^{-1} \mathbf{v}\|. \quad (51)$$

Let  $\mathbf{L} = \mathbf{V} \mathbf{\Lambda} \mathbf{V}^\top$  be the eigenvalue decomposition of the Laplacian matrix, where  $\mathbf{V}$  is unitary and  $\mathbf{\Lambda}$  is diagonal. Since  $\mathbf{L} \cdot \mathbf{1} = \mathbf{0}$ , the first column of  $\mathbf{V}$  equals  $\mathbf{1}_N / \sqrt{N}$  and  $[\mathbf{\Lambda}]_{1,1} = 0$ ; furthermore,  $[\mathbf{\Lambda}]_{i,i} \geq \rho_2 > 0, \forall i > 1$  (Assumption 4). Then,  $\hat{\mathbf{L}} = \mathbf{L} \otimes \mathbf{I}_d = \hat{\mathbf{V}} \hat{\mathbf{\Lambda}} \hat{\mathbf{V}}^\top$ , where  $\hat{\mathbf{V}} = \mathbf{V} \otimes \mathbf{I}_d$  and  $\hat{\mathbf{\Lambda}} = \mathbf{\Lambda} \otimes \mathbf{I}_d$ . Let

$$\tilde{\mathbf{A}} = \hat{\mathbf{V}}^\top \mathbf{A} \hat{\mathbf{V}} = \begin{bmatrix} \tilde{\mathbf{A}}_{1,1} & \tilde{\mathbf{A}}_{1,2} \\ \tilde{\mathbf{A}}_{1,2}^\top & \tilde{\mathbf{A}}_{2,2} \end{bmatrix}, \quad \hat{\mathbf{\Lambda}} = \begin{bmatrix} \mathbf{0} & \mathbf{0} \\ \mathbf{0} & \hat{\mathbf{\Lambda}}_{2,2} \end{bmatrix},$$

where  $\tilde{\mathbf{A}}_{1,1} \in \mathbb{R}^{d \times d}$ ,  $\tilde{\mathbf{A}}_{1,2} \in \mathbb{R}^{d \times (N-1)d}$ ,  $\tilde{\mathbf{A}}_{2,2}$  and  $\hat{\mathbf{\Lambda}}_{2,2} \in \mathbb{R}^{(N-1)d \times (N-1)d}$  with  $\hat{\mathbf{\Lambda}}_{2,2} \succeq \rho_2 \mathbf{I}$ . Since  $\mathbf{v} \perp (\mathbf{1}_N \otimes \mathbf{I}_d)$ , we also define  $\hat{\mathbf{V}}^\top \mathbf{v} = [\mathbf{0}^\top, \mathbf{x}^\top]^\top$  for suitable  $\mathbf{x}$ . Therefore,

$$\|\mathbf{A} \mathbf{B}^{-1} \mathbf{v}\| = \|\tilde{\mathbf{A}} (\tilde{\mathbf{A}} + U \hat{\mathbf{\Lambda}})^{-1} \begin{bmatrix} \mathbf{0} \\ \mathbf{x} \end{bmatrix}\|.$$

Using the inversion properties of  $2 \times 2$  block matrices and simplifying, we continue as  $\|\mathbf{A} \mathbf{B}^{-1} \mathbf{v}\|$

$$= \left\| \begin{bmatrix} \tilde{\mathbf{A}}_{1,1} & \tilde{\mathbf{A}}_{1,2} \\ \tilde{\mathbf{A}}_{1,2}^\top & \tilde{\mathbf{A}}_{2,2} \end{bmatrix} \begin{bmatrix} \bullet & -\tilde{\mathbf{A}}_{1,1}^{-1} \tilde{\mathbf{A}}_{1,2} \mathbf{S}_U^{-1} \\ \bullet & \mathbf{S}_U^{-1} \end{bmatrix} \begin{bmatrix} \mathbf{0} \\ \mathbf{x} \end{bmatrix} \right\| = \|\mathbf{S}_0 \mathbf{S}_U^{-1} \mathbf{x}\|,$$

where  $\mathbf{S}_z \triangleq \tilde{\mathbf{A}}_{2,2} - \tilde{\mathbf{A}}_{1,2}^\top \tilde{\mathbf{A}}_{1,1}^{-1} \tilde{\mathbf{A}}_{1,2} + z \hat{\mathbf{\Lambda}}$  is the Schur complement of block  $\tilde{\mathbf{A}}_{1,1}$  of  $\tilde{\mathbf{A}} + z \hat{\mathbf{\Lambda}}$ , and the block elements  $\bullet$  are irrelevant, being then multiplied by  $\mathbf{0}$ . Using the facts that  $\mathbf{0} \prec \mathbf{S}_0 \leq L \cdot \mathbf{I}$  ( $\mathbf{S}_0^{-1}$  is the lower-diagonal block of  $\tilde{\mathbf{A}}^{-1}$ , and  $\tilde{\mathbf{A}}^{-1} \succeq \frac{1}{L} \mathbf{I}$ ) and  $\mathbf{S}_U = \mathbf{S}_0 + U \hat{\mathbf{\Lambda}} \succeq U \rho_2 \mathbf{I}$ , yield

$$\|\mathbf{A} \mathbf{B}^{-1} \mathbf{v}\| = \|\mathbf{S}_0 \mathbf{S}_U^{-1} \mathbf{x}\| \leq L \|\mathbf{S}_U^{-1} \mathbf{x}\| \leq \frac{L}{U \rho_2} \|\mathbf{x}\| = \frac{L}{U \rho_2} \|\mathbf{v}\|.$$

The final result is obtained by using this bound in (51).  $\square$

**Lemma 4.**  $\|\hat{\mathbf{L}} \mathbf{W}_k^*\| \leq \frac{\eta_k}{\gamma_k} \sqrt{N} \nabla^* \left(1 + \frac{L^2}{\mu \rho_2} \frac{\eta_k}{\gamma_k}\right), \forall k \geq \bar{k}$ .

*Proof.* From the proof of (29) in Appendix B.II,  $\nabla G_k(\mathbf{W}_k^*) = \nabla f(\mathbf{W}_k^*) + \frac{\gamma_k}{\eta_k} \hat{\mathbf{L}} \mathbf{W}_k^* = \mathbf{0}$  for  $k \geq \bar{k}$  (see (45)). It follows that

$$\|\hat{\mathbf{L}} \mathbf{W}_k^*\| = \frac{\eta_k}{\gamma_k} \|\nabla f(\mathbf{W}_k^*)\|.$$

Moreover, using the triangle inequality and smoothness of  $f$ ,

$$\begin{aligned} \|\nabla f(\mathbf{W}_k^*)\| &\leq \|\nabla f(\mathbf{W}_k^*) - \nabla f(\mathbf{W}^*)\| + \|\nabla f(\mathbf{W}^*)\| \\ &\leq L \|\mathbf{W}_k^* - \mathbf{W}^*\| + \|\nabla f(\mathbf{W}^*)\|. \end{aligned}$$

The final result is obtained by bounding  $\|\mathbf{W}_k^* - \mathbf{W}^*\|$  as in (29), and  $\|\nabla f(\mathbf{W}^*)\| \leq \sqrt{N} \nabla^*$ .  $\square$

## APPENDIX C: PROOF OF THEOREM 2

*Proof.* First, note that the choice of stepsizes guarantees the existence of  $\bar{k} \geq 0$  (finite) such that **C1-C3** are satisfied for  $k \geq \bar{k}$ . Consider  $k \geq \bar{k}$ . In the proof, we will often need

$$S_k^n(v) \triangleq \delta \sum_{t=\bar{k}}^{k-1} P_{t+1,k}^n (t+\delta)^{-v}, \quad \text{for } 1 \leq v \leq \frac{5}{4}n \text{ and } n \geq 1.$$

Using  $P_{t,k} = \prod_{j=t}^{k-1} (1 - \mu \eta_j) \leq e^{-\mu \eta_0 \delta \sum_{j=t}^{k-1} (j+\delta)^{-1}} \leq e^{-\mu \eta_0 \delta \int_t^k (x+\delta)^{-1} dx} = (k+\delta)^{-\mu \eta_0 \delta} (t+\delta)^{\mu \eta_0 \delta}$ ,

we can bound  $S_k^n(v)$

$\leq \delta (k+\delta)^{-n \mu \eta_0 \delta} (1 + 1/(\bar{k} + \delta))^{n \mu \eta_0 \delta} \sum_{t=\bar{k}}^{k-1} (t+\delta)^{n \mu \eta_0 \delta - v}$  and since  $n \mu \eta_0 \delta \geq 5/4n \geq v$  and  $(1 + 1/(\bar{k} + \delta))^{n \mu \eta_0 \delta} \leq e^{n \mu \eta_0 \delta / (\bar{k} + \delta)} = e^{n \mu \eta_{\bar{k}}} \leq e^n$  (note that  $\eta_{\bar{k}} \leq 2/(\mu + L) \leq 1/\mu$  from **C1** of Theorem 1), we proceed as

$$\begin{aligned} S_k^n(v) &\leq \delta (k+\delta)^{-n \mu \eta_0 \delta} e^n \int_{\bar{k}}^k (x+\delta)^{n \mu \eta_0 \delta - v} dx \\ &\leq \frac{e^n \delta}{n \mu \eta_0 \delta - v + 1} (k+\delta)^{-v+1} \leq e^n \frac{5}{4 \mu \eta_0} (k+\delta)^{-v+1}, \quad (52) \end{aligned}$$

where the last step used  $\delta \geq 5/(4 \mu \eta_0)$ ,  $v \leq 5/4n$ . With  $\gamma_k, \eta_k$  as in Theorem 2, we specialize (27) as

$$\frac{1}{N} \|\mathbf{W}_k - \tilde{\mathbf{W}}_k\|_{\mathbb{E}}^2 \leq \gamma_0^2 \delta^{1/2} \Sigma^{(1)} S_k^2(3/2) + \eta_0^2 \delta \Sigma^{(2)} S_k^2(2);$$

(34) follows using (52) and  $\sqrt{a+b} \leq \sqrt{a} + \sqrt{b}$  for  $a, b \geq 0$ . Similarly, we specialize (28) as

$$\begin{aligned} \frac{1}{\sqrt{N}} \|\tilde{\mathbf{W}}_k - \mathbf{W}_k^*\|_{\mathbb{E}} &\leq \text{dm}(\mathcal{W}) \cdot P_{\bar{k},k} - \frac{\nabla^* L}{\mu \rho_2} \frac{\eta_0 \delta^{1/4}}{\gamma_0} \sum_{t=\bar{k}}^{k-1} P_{t+1,k} \\ &\times \left(1 + \frac{L^2}{\mu \rho_2} \frac{\eta_0 \delta^{1/4}}{\gamma_0} (t+\delta)^{-1/4}\right) \left((t+1+\delta)^{-1/4} - (t+\delta)^{-1/4}\right) \end{aligned}$$

Since  $x^{-1/4}$  is convex for  $x > 0$ , we further bound  $(t+1+\delta)^{-1/4} \geq (t+\delta)^{-1/4} - 1/4(t+\delta)^{-5/4}$ , hence

$$\begin{aligned} \frac{1}{\sqrt{N}} \|\tilde{\mathbf{W}}_k - \mathbf{W}_k^*\|_{\mathbb{E}} &\leq \text{dm}(\mathcal{W}) \cdot P_{\bar{k},k} + \frac{\nabla^* L}{4 \mu \rho_2} \frac{\eta_0 \delta^{-3/4}}{\gamma_0} \\ &\times \left(S_k^1(5/4) + \frac{L^2}{\mu \rho_2} \frac{\eta_0 \delta^{1/4}}{\gamma_0} S_k^1(3/2)\right). \end{aligned}$$

(35) readily follows using (52) and  $\delta \geq \frac{5}{4 \mu \eta_0}$ . (36) follows by direct substitution into (29).  $\square$

## REFERENCES

- [1] N. Michelusi, "Decentralized federated learning via non-coherent over-the-air consensus," in *ICC 2023 - IEEE International Conference on Communications*, 2023, pp. 3102–3107.

- [2] —, “Csi-free over-the-air decentralized learning over frequency selective channels,” in *ICASSP 2024 - 2024 IEEE International Conference on Acoustics, Speech and Signal Processing (ICASSP)*, 2024, pp. 13 076–13 080.
- [3] S. Kar and J. M. Moura, “Consensus + innovations distributed inference over networks: cooperation and sensing in networked systems,” *IEEE Signal Processing Magazine*, vol. 30, no. 3, pp. 99–109, 2013.
- [4] A. Nedić, J.-S. Pang, G. Scutari, and Y. Sun, *Multi-agent Optimization*, 1st ed. Springer, Cham, 2018.
- [5] T. Yang, X. Yi, J. Wu, Y. Yuan, D. Wu, Z. Meng, Y. Hong, H. Wang, Z. Lin, and K. H. Johansson, “A survey of distributed optimization,” *Annual Reviews in Control*, vol. 47, pp. 278–305, 2019.
- [6] G. Zhu, Y. Wang, and K. Huang, “Broadband Analog Aggregation for Low-Latency Federated Edge Learning,” *IEEE Transactions on Wireless Communications*, vol. 19, no. 1, pp. 491–506, 2020.
- [7] X. Lian, C. Zhang, H. Zhang, C.-J. Hsieh, W. Zhang, and J. Liu., “Can decentralized algorithms outperform centralized algorithms? A case study for decentralized parallel stochastic gradient descent,” in *Proc. 31st NeurIPS*, Dec. 2017.
- [8] Y. Xiao, Y. Ye, S. Huang, L. Hao, Z. Ma, M. Xiao, S. Mumtaz, and O. A. Dobre, “Fully Decentralized Federated Learning-Based On-Board Mission for UAV Swarm System,” *IEEE Communications Letters*, vol. 25, no. 10, pp. 3296–3300, 2021.
- [9] S. Savazzi, M. Nicoli, and V. Rampa, “Federated learning with cooperating devices: A consensus approach for massive iot networks,” *IEEE Internet of Things Journal*, vol. 7, no. 5, pp. 4641–4654, 2020.
- [10] A. Nedić and A. Ozdaglar, “Distributed subgradient methods for multi-agent optimization,” *IEEE Trans. Autom. Control*, vol. 54, no. 1, pp. 48–61, Jan. 2009.
- [11] K. Yuan, Q. Ling, and W. Yin, “On the Convergence of Decentralized Gradient Descent,” *SIAM Journal on Optimization*, vol. 26, no. 3, pp. 1835–1854, 2016.
- [12] R. Xin, S. Pu, A. Nedic, and U. A. Khan, “A general framework for decentralized optimization with first-order methods,” *Proceedings of the IEEE*, vol. 108, no. 11, pp. 1869–1889, 2020.
- [13] K. Yang, T. Jiang, Y. Shi, and Z. Ding, “Federated learning via over-the-air computation,” *IEEE Transactions on Wireless Communications*, vol. 19, no. 3, pp. 2022–2035, 2020.
- [14] M. M. Amiri and D. Gündüz, “Federated learning over wireless fading channels,” *IEEE Transactions on Wireless Communications*, vol. 19, no. 5, pp. 3546–3557, 2020.
- [15] M. M. Amiri, D. Gündüz, S. R. Kulkarni, and H. V. Poor, “Convergence of federated learning over a noisy downlink,” *IEEE Transactions on Wireless Communications*, vol. 21, no. 3, pp. 1422–1437, 2022.
- [16] M. M. Amiri, T. M. Duman, D. Gündüz, S. R. Kulkarni, and H. V. Poor, “Blind federated edge learning,” *IEEE Transactions on Wireless Communications*, vol. 20, no. 8, pp. 5129–5143, 2021.
- [17] M. Mohammadi Amiri and D. Gündüz, “Machine learning at the wireless edge: Distributed stochastic gradient descent over-the-air,” *IEEE Transactions on Signal Processing*, vol. 68, pp. 2155–2169, 2020.
- [18] H. Xing, O. Simeone, and S. Bi, “Federated learning over wireless device-to-device networks: Algorithms and convergence analysis,” *IEEE Journal on Selected Areas in Communications*, vol. 39, no. 12, pp. 3723–3741, 2021.
- [19] Y. Shi, Y. Zhou, and Y. Shi, “Over-the-air decentralized federated learning,” in *2021 IEEE International Symposium on Information Theory (ISIT)*, 2021, pp. 455–460.
- [20] E. Ozfatura, S. Rini, and D. Gündüz, “Decentralized sgd with over-the-air computation,” in *GLOBECOM 2020 - 2020 IEEE Global Communications Conference*, 2020, pp. 1–6.
- [21] A. Reiszadeh, A. Mokhtari, H. Hassani, and R. Pedarsani, “An exact quantized decentralized gradient descent algorithm,” *IEEE Transactions on Signal Processing*, vol. 67, no. 19, pp. 4934–4947, 2019.
- [22] H. Xiao, K. Rasul, and R. Vollgraf, “Fashion-mnist: a novel image dataset for benchmarking machine learning algorithms,” *CoRR*, vol. abs/1708.07747, 2017.
- [23] J. Tsitsiklis, D. Bertsekas, and M. Athans, “Distributed asynchronous deterministic and stochastic gradient optimization algorithms,” *IEEE Transactions on Automatic Control*, vol. 31, no. 9, pp. 803–812, 1986.
- [24] H. Taheri, A. Mokhtari, H. Hassani, and R. Pedarsani, “Quantized decentralized stochastic learning over directed graphs,” in *Proc. 37th ICML*, Jul. 2020.
- [25] D. Kovalev, A. Koloskova, M. Jaggi, P. Richtárik, and S. U. Stich, “A linearly convergent algorithm for decentralized optimization: Sending less bits for free!” in *Proc. 24th AISTATS*, Apr. 2021.
- [26] Y. Liao, Z. Li, K. Huang, and S. Pu, “A compressed gradient tracking method for decentralized optimization with linear convergence,” *IEEE Trans. on Automatic Control*, vol. 67, no. 10, pp. 5622–5629, 2022.
- [27] N. Michelusi, G. Scutari, and C.-S. Lee, “Finite-Bit Quantization for Distributed Algorithms With Linear Convergence,” *IEEE Transactions on Information Theory*, vol. 68, no. 11, pp. 7254–7280, 2022.
- [28] Y. Kajiyama, N. Hayashi, and S. Takai, “Linear convergence of consensus-based quantized optimization for smooth and strongly convex cost functions,” *IEEE Transactions on Automatic Control*, vol. 66, no. 3, pp. 1254–1261, 2021.
- [29] S. Magnússon, H. Shokri-Ghadikolaei, and N. Li, “On maintaining linear convergence of distributed learning and optimization under limited communication,” *IEEE Trans. Signal Process.*, vol. 68, pp. 6101–6116, Oct. 2020.
- [30] R. Saha, S. Rini, M. Rao, and A. J. Goldsmith, “Decentralized optimization over noisy, rate-constrained networks: Achieving consensus by communicating differences,” *IEEE Journal on Selected Areas in Communications*, vol. 40, no. 2, pp. 449–467, 2022.
- [31] Z. Jiang, G. Yu, Y. Cai, and Y. Jiang, “Decentralized Edge Learning via Unreliable Device-to-Device Communications,” *IEEE Transactions on Wireless Communications*, vol. 21, no. 11, pp. 9041–9055, 2022.
- [32] H. Ye, L. Liang, and G. Y. Li, “Decentralized Federated Learning With Unreliable Communications,” *IEEE Journal of Selected Topics in Signal Processing*, vol. 16, no. 3, pp. 487–500, 2022.
- [33] E. Jeong, M. Zecchin, and M. Kountouris, “Asynchronous Decentralized Learning over Unreliable Wireless Networks,” in *ICC 2022 - IEEE International Conference on Communications*, 2022, pp. 607–612.
- [34] M. Chen, D. Gündüz, K. Huang, W. Saad, M. Bennis, A. V. Feljan, and H. V. Poor, “Distributed learning in wireless networks: Recent progress and future challenges,” *IEEE Journal on Selected Areas in Communications*, vol. 39, no. 12, pp. 3579–3605, 2021.
- [35] B. Nazer and M. Gastpar, “Computation Over Multiple-Access Channels,” *IEEE Transactions on Information Theory*, vol. 53, no. 10, pp. 3498–3516, 2007.
- [36] J. Choi, “Communication-Efficient Distributed SGD using Random Access for Over-the-Air Computation,” *IEEE Journal on Selected Areas in Information Theory*, pp. 1–1, 2022.
- [37] J. Dong, Y. Shi, and Z. Ding, “Blind Over-the-Air Computation and Data Fusion via Provable Wirtinger Flow,” *IEEE Transactions on Signal Processing*, vol. 68, pp. 1136–1151, 2020.
- [38] T. Sery and K. Cohen, “On Analog Gradient Descent Learning Over Multiple Access Fading Channels,” *IEEE Transactions on Signal Processing*, vol. 68, pp. 2897–2911, 2020.
- [39] V. Gandikota, D. Kane, R. K. Maity, and A. Mazumdar, “vqSGD: Vector Quantized Stochastic Gradient Descent,” *IEEE Transactions on Information Theory*, vol. 68, no. 7, pp. 4573–4587, 2022.
- [40] C.-S. Lee, N. Michelusi, and G. Scutari, “Finite rate distributed weight-balancing and average consensus over digraphs,” *IEEE Transactions on Automatic Control*, vol. 66, no. 10, pp. 4530–4545, 2021.
- [41] M. Chen, H. V. Poor, W. Saad, and S. Cui, “Wireless communications for collaborative federated learning,” *IEEE Communications Magazine*, vol. 58, no. 12, pp. 48–54, 2020.
- [42] F. P.-C. Lin, S. Hosseinalipour, S. S. Azam, C. G. Brinton, and N. Michelusi, “Semi-decentralized federated learning with cooperative d2d local model aggregations,” *IEEE Journal on Selected Areas in Communications*, vol. 39, no. 12, pp. 3851–3869, 2021.
- [43] M. Yemini, R. Saha, E. Ozfatura, D. Gündüz, and A. J. Goldsmith, “Semi-decentralized federated learning with collaborative relaying,” in *2022 IEEE International Symposium on Information Theory (ISIT)*, 2022, pp. 1471–1476.
- [44] S. Hosseinalipour, S. S. Azam, C. G. Brinton, N. Michelusi, V. Aggarwal, D. J. Love, and H. Dai, “Multi-stage hybrid federated learning over large-scale d2d-enabled fog networks,” *IEEE/ACM Transactions on Networking*, vol. 30, no. 4, pp. 1569–1584, 2022.
- [45] J. L. Gross, J. Yellen, and P. Zhang, *Handbook of Graph Theory, Second Edition*, 2nd ed. Chapman & Hall/CRC, 2013.
- [46] S. Wang, T. Tuor, T. Salonidis, K. K. Leung, C. Makaya, T. He, and K. Chan, “Adaptive Federated Learning in Resource Constrained Edge Computing Systems,” *IEEE Journal on Selected Areas in Communications*, vol. 37, no. 6, pp. 1205–1221, 2019.
- [47] I. Florescu and C. A. Tudor, *Handbook of Probability*. Wiley, 2013.
- [48] V. Schwarz, G. Hannak, and G. Matz, “On the convergence of average consensus with generalized metropolis-hasting weights,” in *IEEE International Conference on Acoustics, Speech and Signal Processing (ICASSP)*, 2014, pp. 5442–5446.
- [49] J. Wu, W. Hu, H. Xiong, J. Huan, V. Braverman, and Z. Zhu, “On the Noisy Gradient Descent that Generalizes as SGD,” in *ICML*, 2020.
- [50] D. Bertsekas, A. Nedić, and A. Ozdaglar, *Convex Analysis and Optimization*. Athena Scientific, 2003.

# Supplemental Document

In this supplemental document, we provide the proof of Lemma 1 of the main manuscript. We also provide additional numerical evaluations showcasing the parameters' selection of NCOTA-DGD, as well comparisons with state-of-the-art schemes.

## PROOF OF LEMMA 1

In this section, we provide the proof of Lemma 1, restated below for ease of reference.

**Lemma 1:** Consider channels satisfying Assumption 1. Furthermore, assume the resource units are evenly allocated among  $m = 1, \dots, M$ , i.e.,  $|R_m - Q/M| < 1, \forall m$ . Let:

$$\vartheta \triangleq \max_{i,j \neq i} \frac{1}{\Lambda_{i,j}} \left( \frac{1}{Q} \sum_{q=1}^Q \mathbb{E}[(|\mathbf{h}_{i,j}|_q|^2 - \Lambda_{i,j})^2] \right)^{1/2}, \quad (53)$$

$$\varsigma \triangleq \max_{i,j \neq i} \frac{1}{\Lambda_{i,j}} \left( \frac{1}{M} \sum_{m=1}^M \mathbb{E}[(\hat{\lambda}_{i,j}^{(m)} - \Lambda_{i,j})^2] \right)^{1/2}, \quad (54)$$

$$\Lambda^* \triangleq \max_i \sum_{j \neq i} \Lambda_{i,j}, \quad (55)$$

where  $\hat{\lambda}_{i,j}^{(m)} = \frac{1}{R_m} \sum_{q \in \mathcal{R}_m} |\mathbf{h}_{i,j}|_q|^2$  is the sample average channel gain across the resource units in the set  $\mathcal{R}_m$ . Then,  $\frac{1}{N} \sum_{i=1}^N \text{var}(\tilde{\mathbf{d}}_i) \leq \Sigma^{(1)} \triangleq \max_{\mathbf{z}, \mathbf{z}' \in \mathcal{Z}} \|\mathbf{z} - \mathbf{z}'\|^2$

$\times \frac{1}{1-p_{\text{tx}}} \left[ \frac{\sqrt{M}}{\sqrt{Q}} \sqrt{2(1+2\vartheta^2)} \Lambda^* + \frac{\sqrt{1+\varsigma^2}}{\sqrt{p_{\text{tx}}}} \Lambda^* + \frac{\sqrt{M}}{\sqrt{Q}} \frac{N_0}{E p_{\text{tx}}} \right]^2$ . The value of the transmission probability  $p_{\text{tx}}$  minimizing this bound is the unique solution in  $(0, 1)$  of  $\sqrt{2(1+2\vartheta^2)} \Lambda^* p_{\text{tx}}^{3/2} + \frac{\sqrt{Q}}{\sqrt{M}} \sqrt{1+\varsigma^2} \Lambda^* (2p_{\text{tx}} - 1) + \frac{N_0}{E} \frac{3p_{\text{tx}} - 2}{\sqrt{p_{\text{tx}}}} = 0$ .

*Proof.* We start with

$$\frac{1}{N} \sum_{i=1}^N \text{var}(\tilde{\mathbf{d}}_i) \leq \max_i \text{var}(\tilde{\mathbf{d}}_i) = \max_i (\text{sdv}(\tilde{\mathbf{d}}_i))^2. \quad (56)$$

Hence, we focus on bounding  $\text{sdv}(\tilde{\mathbf{d}}_i)$  for a generic  $i$ . Using (7), we can express

$$\tilde{\mathbf{d}}_i - \mathbb{E}[\tilde{\mathbf{d}}_i] = \sum_{m=1}^M (r_{i,m} - \mathbb{E}[r_{i,m}]) (\mathbf{z}_m - \mathbf{w}_i).$$

Next, we use Minkowski inequality [47, Lemma 14.10],  $\sqrt{\mathbb{E}[\|\sum_m \mathbf{a}_m\|^2]} \leq \sum_m \sqrt{\mathbb{E}[\|\mathbf{a}_m\|^2]}$ . It yields

$$\begin{aligned} \text{sdv}(\tilde{\mathbf{d}}_i) &= \sqrt{\mathbb{E}[\|\tilde{\mathbf{d}}_i - \mathbb{E}[\tilde{\mathbf{d}}_i]\|^2]} \\ &\leq \sum_{m=1}^M \text{sdv}(r_{i,m}) \|\mathbf{z}_m - \mathbf{w}_i\|. \end{aligned} \quad (57)$$

We bound  $\|\mathbf{z}_m - \mathbf{w}_i\|$  by using the fact that  $\mathbf{w}_i = \sum_{m'=1}^M [\mathbf{p}_i]_{m'} \mathbf{z}_{m'}$  and the triangle inequality, yielding

$$\|\mathbf{z}_m - \mathbf{w}_i\| \leq \sum_{m'=1}^M [\mathbf{p}_i]_{m'} \|\mathbf{z}_m - \mathbf{z}_{m'}\|$$

$$\leq \max_{m', m''} \|\mathbf{z}_{m''} - \mathbf{z}_{m'}\| = \max_{\mathbf{z}, \mathbf{z}' \in \mathcal{Z}} \|\mathbf{z} - \mathbf{z}'\|,$$

so that (57) is further upper bounded as

$$\text{sdv}(\tilde{\mathbf{d}}_i) \leq \max_{\mathbf{z}, \mathbf{z}' \in \mathcal{Z}} \|\mathbf{z} - \mathbf{z}'\| \sum_{m=1}^M \text{sdv}(r_{i,m}). \quad (58)$$

We now focus on bounding  $\text{sdv}(r_{i,m}) = \sqrt{\text{var}(r_{i,m})}$ . We use  $\text{var}(X) = \mathbb{E}_A[\text{var}(X|A)] + \text{var}(\mathbb{E}[X|A])$  to express

$$\text{var}(r_{i,m}) = \mathbb{E} \left[ \text{var} \left( r_{i,m} \middle| \varsigma, \chi_{-i}, \chi_i, \mathbf{h} \right) \right] \quad (59)$$

$$+ \text{var} \left( \mathbb{E} [r_{i,m} | \varsigma, \chi_{-i}, \chi_i, \mathbf{h}] \right). \quad (60)$$

The first variance term captures the impact of the AWGN noise and random phase injected at the transmitters; the second term captures the impact of the randomness in the channels ( $\mathbf{h}$ ), circular shift ( $\varsigma$ ), random transmission of node  $i$  ( $\chi_i$ ) and of all other nodes ( $\chi_{-i}$ ). Next, we bound each variance term individually.

Bounding  $\mathbb{E}[\text{var}(r_{i,m} | \varsigma, \chi_{-i}, \chi_i, \mathbf{h})]$ : Let  $m' \triangleq m \oplus \varsigma$  and

$$\begin{aligned} A_q &\triangleq \sum_{j \neq i} \chi_j |\mathbf{h}_{i,j}|_q [\mathbf{x}_j]_q \\ &= \sqrt{\frac{EQ}{R_{m'}}} \sum_{j \neq i} \chi_j e^{j[\theta_j]_q} |\mathbf{h}_{i,j}|_q \sqrt{[\mathbf{p}_j]_m}, \quad \forall q \in \mathcal{R}_{m'}. \end{aligned}$$

Then, we can express  $[\mathbf{y}_i]_q = A_q + [\mathbf{n}_i]_q$  and

$$r_{i,m} = \frac{1 - \chi_i}{EQ p_{\text{tx}} (1 - p_{\text{tx}})} \sum_{q \in \mathcal{R}_{m'}} (|A_q + [\mathbf{n}_i]_q|^2 - N_0).$$

Note that, when conditioned on  $\varsigma, \chi_{-i}, \chi_i, \mathbf{h}$  (hence on  $m'$ ), the terms  $|A_q + [\mathbf{n}_i]_q|^2$  are independent across  $q$ , due to independence of  $[\mathbf{n}_i]_q$ , and of the phases  $[\theta_j]_q$  across  $q \in \mathcal{R}_{m'}$  and  $j$ . Therefore,

$$\begin{aligned} \text{var}(r_{i,m} | \varsigma, \chi_{-i}, \chi_i, \mathbf{h}) &= \frac{1 - \chi_i}{E^2 Q^2 p_{\text{tx}}^2 (1 - p_{\text{tx}})^2} \\ &\times \sum_{q \in \mathcal{R}_{m'}} \text{var}(|A_q + [\mathbf{n}_i]_q|^2 | \varsigma, \chi_{-i}, \mathbf{h}). \end{aligned} \quad (61)$$

Using the independence of the noise and of the phases injected at the transmitters (across transmitters  $j$ ), the fact that  $\mathbb{E}[e^{j[\theta_{j_1} - \theta_{j_2} + \theta_{j_3} - \theta_{j_4}]_q}] = \mathbb{1}[j_3 = j_4, j_1 = j_2] + \mathbb{1}[j_3 = j_2, j_4 = j_1, j_1 \neq j_2]$ , and  $\mathbb{E}[\|\mathbf{n}_i\|_q^4] = 2N_0^2$ , we find that

$$\begin{aligned} \text{var}(|A_q + [\mathbf{n}_i]_q|^2 | \varsigma, \chi_{-i}, \mathbf{h}) &= \frac{EQ}{R_{m'}} \sum_{j \neq i} \chi_j |\mathbf{h}_{i,j}|_q^2 [\mathbf{p}_j]_m \\ &\times \left( \frac{EQ}{R_{m'}} \sum_{j' \neq i, j} \chi_{j'} |\mathbf{h}_{i,j'}|_q^2 [\mathbf{p}_{j'}]_m + 2N_0 \right) + N_0^2. \end{aligned}$$

Next, we compute the expectation of this variance term with respect to the random transmission of nodes  $j \neq i$ . Since these are independent across  $j \neq j'$  and occur with probability  $p_{\text{tx}}$ ,



we obtain

$$\begin{aligned} & \mathbb{E}_{\chi_{-i}}[\text{var}(|A_{s,q} + [\mathbf{n}_i^{(s)}]_q|^2 | \varsigma, \chi_{-i}, \mathbf{h})] \\ &= \left( \frac{EQp_{\text{tx}}}{R_{m'}} \sum_{j \neq i} |\mathbf{h}_{i,j}|_q|^2 [\mathbf{p}_j]_m + N_0 \right)^2 \\ & \quad - \frac{(EQp_{\text{tx}})^2}{(R_{m'})^2} \sum_{j \neq i} |\mathbf{h}_{i,j}|_q|^4 [\mathbf{p}_j]_m^2. \end{aligned}$$

Substituting in the expression of  $\text{var}(r_{i,m} | \varsigma, \chi_{-i}, \chi_i, \mathbf{h})$  in (61), discarding the negative term above, and further taking the expectation with respect to the transmission indicator  $\chi_i \in \{0, 1\}$ , the circular shift  $\varsigma$  (hence  $m' = m \oplus \varsigma$  becomes uniform in  $\{1, \dots, M\}$ ), and the channels, yields

$$\begin{aligned} \mathbb{E}[\text{var}(r_{i,m} | \varsigma, \chi_{-i}, \chi_i, \mathbf{h})] &= \frac{1}{E^2 Q^2 p_{\text{tx}}^2 (1 - p_{\text{tx}})} \\ & \times \frac{1}{M} \sum_{m', q} \mathbb{E}_{\mathbf{h}} \left[ \left( \frac{EQp_{\text{tx}}}{R_{m'}} \sum_{j \neq i} |\mathbf{h}_{i,j}|_q|^2 [\mathbf{p}_j]_m + N_0 \right)^2 \right], \quad (62) \end{aligned}$$

where we defined the shorthand notation  $\sum_{m', q} \equiv \sum_{m'=1}^M \sum_{q \in \mathcal{R}_{m'}}$ . The term above has the form

$$\sum_t \mathbb{E} \left[ \left( \sum_j \alpha_{j,t} \right)^2 \right]$$

for suitable  $\alpha_{j,t}$ . We can upper bound it as

$$\begin{aligned} &= \sum_{j', j} \sum_t \mathbb{E}[\alpha_{j,t} \alpha_{j',t}] \leq \sum_{j', j} \sum_t \sqrt{\mathbb{E}[\alpha_{j,t}^2]} \sqrt{\mathbb{E}[\alpha_{j',t}^2]} \\ &\leq \sum_{j', j} \sqrt{\sum_t \mathbb{E}[\alpha_{j,t}^2]} \sqrt{\sum_t \mathbb{E}[\alpha_{j',t}^2]} = \left( \sum_j \sqrt{\sum_t \mathbb{E}[\alpha_{j,t}^2]} \right)^2, \end{aligned}$$

where in the first step we used Holder's inequality, in the second step we used Cauchy-Schwarz inequality. Using this bound in (62) yields

$$\begin{aligned} & \mathbb{E}[\text{var}(r_{i,m} | \varsigma, \mathcal{T}_{-i}, \tau_i, \mathbf{h})] \\ & \leq \frac{1}{1 - p_{\text{tx}}} \left( \sum_{j \neq i} \sqrt{\sum_{m', q} \frac{1}{MR_{m'}^2} \mathbb{E}[|\mathbf{h}_{i,j}|_q|^4] [\mathbf{p}_j]_m} \right. \\ & \quad \left. + \frac{N_0}{\sqrt{MQE} p_{\text{tx}}} \right)^2. \quad (63) \end{aligned}$$

We further bound

$$\begin{aligned} & \sum_{m', q} \frac{1}{MR_{m'}^2} \mathbb{E}[|\mathbf{h}_{i,j}|_q|^4] \leq \frac{2M}{Q} \sum_{m', q} \frac{1}{MR_{m'}} \mathbb{E}[|\mathbf{h}_{i,j}|_q|^4] \\ &= \frac{2M}{Q} \left( \sum_{m'=1}^M \sum_{q \in \mathcal{R}_{m'}} \frac{1}{MR_{m'}} \mathbb{E}[ (|\mathbf{h}_{i,j}|_q|^2 - \Lambda_{i,j})^2 ] + \Lambda_{i,j}^2 \right) \\ &\leq \frac{2M}{Q} \left( \frac{2}{Q} \sum_{q=1}^Q \mathbb{E}[ (|\mathbf{h}_{i,j}|_q|^2 - \Lambda_{i,j})^2 ] + \Lambda_{i,j}^2 \right) \\ &\leq \frac{2M}{Q} (1 + 2\vartheta^2) \Lambda_{i,j}^2, \end{aligned}$$

where in the first and third steps we used  $1/R_{m'} \leq 2M/Q$  (a consequence of the uniform allocation of resource units), in

the second step we used the fact that (Assumption 1)

$$\frac{1}{R_{m'}} \sum_{q \in \mathcal{R}_{m'}} \mathbb{E}[|\mathbf{h}_{i,j}|_q|^2] = \Lambda_{i,j}^{(m')}, \quad \Lambda_{i,j} = \frac{1}{M} \sum_{m'=1}^M \Lambda_{i,j}^{(m')},$$

and in the last step we used (53). Substituting this bound in (63) yields

$$\begin{aligned} & \mathbb{E}[\text{var}(r_{i,m} | \varsigma, \chi_{-i}, \chi_i, \mathbf{h})] \\ & \leq \frac{M}{Q(1 - p_{\text{tx}})} \left( \sqrt{2(1 + 2\vartheta^2)} \sum_{j \neq i} \Lambda_{i,j} [\mathbf{p}_j]_m + \frac{N_0}{EMp_{\text{tx}}} \right)^2. \end{aligned}$$

Bounding  $\text{var}(\mathbb{E}[r_{i,m} | \varsigma, \chi_{-i}, \chi_i, \mathbf{h}])$ : Note that

$$\text{var}(\mathbb{E}[r_{i,m} | \varsigma, \chi_{-i}, \chi_i, \mathbf{h}]) \leq \mathbb{E}[\mathbb{E}[r_{i,m} | \varsigma, \chi_{-i}, \chi_i, \mathbf{h}]^2]. \quad (64)$$

From (14) and (4),

$$\mathbb{E}[r_{i,m} | \varsigma, \chi_{-i}, \chi_i, \mathbf{h}] = (1 - \chi_i) \frac{\sum_{j \neq i} \chi_j \hat{\lambda}_{i,j}^{(m')} [\mathbf{p}_j]_m}{p_{\text{tx}} (1 - p_{\text{tx}})} \quad (65)$$

where  $\hat{\lambda}_{i,j}^{(m')} = \frac{1}{R_{m'}} \sum_{q \in \mathcal{R}_{m'}} |\mathbf{h}_{i,j}|_q|^2$  is the sample average gain across the resource units in the set  $\mathcal{R}_{m'}$ . We square and take the expectation with respect to  $(\varsigma, \chi_{-i}, \chi_i, \mathbf{h})$ , yielding

$$\begin{aligned} \mathbb{E}[\mathbb{E}[r_{i,m} | \varsigma, \chi_{-i}, \chi_i, \mathbf{h}]^2] &= \frac{\mathbb{E}[(\sum_{j \neq i} \chi_j \hat{\lambda}_{i,j}^{(m')} [\mathbf{p}_j]_m)^2]}{p_{\text{tx}}^2 (1 - p_{\text{tx}})} \\ &\leq \frac{\left( \sum_{j \neq i} \sqrt{\mathbb{E}[\chi_j (\hat{\lambda}_{i,j}^{(m')})^2]} [\mathbf{p}_j]_m \right)^2}{p_{\text{tx}}^2 (1 - p_{\text{tx}})} \quad (66) \end{aligned}$$

where in the last step we used Holder's inequality  $\mathbb{E}[AB] = \sqrt{\mathbb{E}[A^2]} \sqrt{\mathbb{E}[B^2]}$  with the random variables  $A = \chi_j \hat{\lambda}_{i,j}^{(m')}$  and  $B = \chi_{j'} \hat{\lambda}_{i,j'}$ . Furthermore,

$$\mathbb{E}[\chi_j (\hat{\lambda}_{i,j}^{(m')})^2] = \frac{p_{\text{tx}}}{M} \sum_{m'=1}^M \mathbb{E}[(\hat{\lambda}_{i,j}^{(m')})^2]$$

where we computed the expectation with respect to the transmission indicator and the circular shift  $\varsigma$  (hence  $m' = m \oplus \varsigma$  uniform in  $\{1, \dots, M\}$ ). We continue as

$$\begin{aligned} \mathbb{E}[\chi_j (\hat{\lambda}_{i,j}^{(m')})^2] &= p_{\text{tx}} \left( \frac{1}{M} \sum_{m'=1}^M \mathbb{E}[(\hat{\lambda}_{i,j}^{(m')} - \Lambda_{i,j})^2] + \Lambda_{i,j}^2 \right) \\ &\leq p_{\text{tx}} (1 + \varsigma^2) \Lambda_{i,j}^2, \end{aligned}$$

where we used the fact that  $\frac{1}{M} \mathbb{E}[\hat{\lambda}_{i,j}^{(m')}] = \Lambda_{i,j}^{(m')}$  and  $\Lambda_{i,j} = \frac{1}{M} \sum_{m'=1}^M \Lambda_{i,j}^{(m')}$ , followed by (54). Substituting this bound into (66) and then in (64) yields

$$\mathbb{E}[\text{var}(r_{i,m} | \varsigma, \mathcal{T}_{-i}, \tau_i, \mathbf{h})] \leq \frac{1 + \varsigma^2}{p_{\text{tx}} (1 - p_{\text{tx}})} \left( \sum_{j \neq i} \Lambda_{i,j} [\mathbf{p}_j]_m \right)^2.$$

Final results: Combining the results together into (59) yields

$$\begin{aligned} \text{var}(r_{i,m}) &\leq \frac{1 + \varsigma^2}{p_{\text{tx}} (1 - p_{\text{tx}})} \left( \sum_{j \neq i} \Lambda_{i,j} [\mathbf{p}_j]_m \right)^2 \\ & \quad + \frac{M}{Q(1 - p_{\text{tx}})} \left( \sqrt{2(1 + 2\vartheta^2)} \sum_{j \neq i} \Lambda_{i,j} [\mathbf{p}_j]_m + \frac{N_0}{EMp_{\text{tx}}} \right)^2. \end{aligned}$$

Finally, we take the square root of both sides, along with

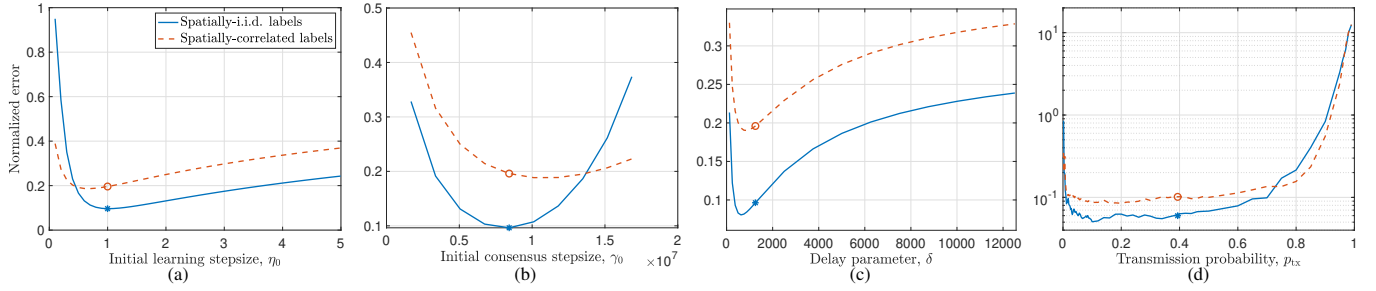


Fig. 5: Normalized error vs initial learning stepsize (a), initial consensus stepsize (b), delay parameter  $\delta$  (c), and transmission probability  $p_{\text{tx}}$  (d), evaluated after 2000ms of execution time, under spatially-i.i.d. (solid lines) and -correlated (dashed lines) scenarios, with i.i.d. channels over frames. The markers denote the *Baseline* configuration, adopted in Sec. V:  $\eta_0 = \frac{2}{\mu+L}$ ,  $\gamma_0 = \frac{0.05}{\rho^2}$ ,  $\delta = \frac{5}{4\mu\eta_0}$ ,  $p_{\text{tx}}$  as in Lemma 1. The common legend is shown in figure (a).

$\sqrt{\sum_{\ell} a_{\ell}^2} \leq \sum_{\ell} a_{\ell}$  for  $a_i \geq 0$ , add over  $m$  and use the fact that  $\sum_m [\mathbf{p}_j]_m = 1$ . These steps yield

$$\begin{aligned} \sum_{m=1}^M \text{sdv}(r_{i,m}) &\leq \frac{\sqrt{M}}{\sqrt{Q}\sqrt{1-p_{\text{tx}}}} \sqrt{2(1+2\vartheta^2)} \sum_{j \neq i} \Lambda_{i,j} \\ &+ \frac{\sqrt{M}}{\sqrt{Q}\sqrt{1-p_{\text{tx}}}} \frac{N_0}{E p_{\text{tx}}} + \frac{\sqrt{1+\varsigma^2}}{\sqrt{p_{\text{tx}}}\sqrt{1-p_{\text{tx}}}} \sum_{j \neq i} \Lambda_{i,j} \triangleq g(p_{\text{tx}}). \end{aligned}$$

The final result is obtained by using the previous bound in (58), along with  $\sum_{j \neq i} \Lambda_{i,j} \leq \Lambda^*$  (see (55)). Finally, it is straightforward to show that  $\lim_{p_{\text{tx}} \rightarrow 0} g(p_{\text{tx}}) = \infty$ ,  $\lim_{p_{\text{tx}} \rightarrow 1} g(p_{\text{tx}}) = \infty$ , and

$$g'(p_{\text{tx}}) \propto A p_{\text{tx}}^{3/2} + B(2p_{\text{tx}} - 1) + C \frac{3p_{\text{tx}} - 2}{\sqrt{p_{\text{tx}}}} \triangleq h(p_{\text{tx}})$$

where  $A = \frac{\sqrt{M}}{\sqrt{Q}} \sqrt{2(1+2\vartheta^2)} \Lambda^*$ ,  $B = \sqrt{1+\varsigma^2} \Lambda^*$ ,  $C = \frac{\sqrt{M}}{\sqrt{Q}} \frac{N_0}{E}$ . The function  $h(p_{\text{tx}})$  is decreasing in  $p_{\text{tx}}$  (with  $\lim_{p_{\text{tx}} \rightarrow 0} h(p_{\text{tx}}) = -\infty$ ,  $h(1) = A+B+C$ , hence there exists a unique  $p_{\text{tx}}^* \in (0, 1)$  such that  $h(p_{\text{tx}}^*) = 0$ , hence  $g'(p_{\text{tx}}^*) = 0$ . Such  $p_{\text{tx}}^*$  minimizes  $g(p_{\text{tx}})$ , hence the upper bound  $\Sigma^{(1)}$  on  $\frac{1}{N} \sum_{i=1}^N \text{var}(\hat{\mathbf{d}}_i)$ .  $\square$

#### PERFORMANCE OF NCOTA-DGD WITH RESPECT TO STEPSIZE PARAMETERS AND TRANSMISSION PROBABILITY

In this section, we provide additional numerical evaluations to Sec. V. The simulation parameters and algorithm descriptions are provided in Sec. V.

We evaluate the performance of NCOTA-DGD in terms of its normalized error after 2000ms of execution time, for a network with  $N = 200$  nodes. We use the CP0 codebook of Example 1 with  $M=2d+1=901$  codewords, requiring two OFDM symbols ( $Q=1024$ ), and yielding a frame of duration  $T=2T_{\text{ofdm}}=258\mu\text{s}$ . It follows Algorithm 1.

In Fig. 5, we plot the normalized error versus some key parameters of NCOTA-DGD: the initial learning stepsize  $\eta_0$  (a), the initial consensus stepsize  $\gamma_0$  (b), the delay parameter  $\delta$  (c), and the transmission probability  $p_{\text{tx}}$  (d). To this end, we vary one such parameter, while setting the other parameters equal to the *Baseline* configuration. The latter adopts  $\eta_0 = \frac{2}{\mu+L}$ ,  $\gamma_0 = \frac{0.05}{\rho^2}$ ,  $\delta = \frac{5}{4\mu\eta_0}$ ,  $p_{\text{tx}}$  as in Lemma 1. For instance, Fig. 5.a is obtained by varying  $\eta_0$ , while setting the  $\gamma_0$ ,  $\delta$  and  $p_{\text{tx}}$  parameters as their baseline values.

In Fig. 5.a, we plot the normalized error versus the initial learning stepsize  $\eta_0$ . As expected, tuning of  $\eta_0$  regulates the magnitude of gradient steps, hence the learning progress. A

smaller  $\eta_0$  slows down the progress of the algorithm, resulting in slower convergence and higher normalized error. On the other hand, if the stepsize is too large, the optimization algorithm might oscillate around the minimizer or even diverge away from it. Note that the baseline value  $\eta_0 = \frac{2}{\mu+L}$  (denoted with markers) is the maximum stepsize that guarantees convergence of gradient descent, for the class of strongly-convex and smooth loss functions.

In Fig. 5.b, we plot the normalized error versus the initial consensus stepsize  $\gamma_0$ . As explained in the discussion following Theorem 2, tuning  $\gamma_0$  reflects a delicate balance between speeding up information propagation (favored by larger  $\gamma_0$ ) and minimizing error propagation (smaller  $\gamma_0$ ). This trade-off is in line with the behavior observed in the figure.

In Fig. 5.c, we plot the normalized error versus the delay parameter  $\delta$ . As explained in the discussion following Theorem 2, the choice  $\delta = \frac{5}{4\mu\eta_0}$  is the one that minimizes the convergence bounds stated in Theorem 2, hence the value  $\delta = \frac{5}{4\mu\eta_0}$  is employed in the numerical evaluations of Sec. V. Remarkably, the plots of 5.c demonstrate the same monotonic behavior expected from Theorem 2 in the regime  $\delta \geq \frac{5}{4\mu\eta_0}$ . They also demonstrate that, if the condition  $\delta \geq \frac{5}{4\mu\eta_0}$  of Theorem 2 is violated, the normalized error quickly diverges, since the stepsizes becomes too small too quickly. This numerical evaluation further motivates the use of decreasing vs constant ( $\delta \rightarrow \infty$ ) stepsizes developed in this paper.

In Fig. 5.d, we plot the normalized error versus the transmission probability  $p_{\text{tx}}$ . We remind that the baseline value shown with markers is the one given by Lemma 1 and used in the numerical evaluations of Sec. V. This value minimizes the upper bound on the variance of the disagreement signal estimate, given in Lemma 1. Indeed, Fig. 5.d confirms that the optimal  $p_{\text{tx}}$  value found via Lemma 1 attains nearly optimal numerical performance. Furthermore, the normalized error exhibits a mild dependence with respect to  $p_{\text{tx}}$  around such optimal value, and quickly diverges as  $p_{\text{tx}} \rightarrow 0$  (the transmissions are too sporadic) or  $p_{\text{tx}} \rightarrow 1$  (each node operates as a receiver too infrequently).

#### ADDITIONAL COMPARISONS WITH STATE-OF-THE-ART SCHEMES

Fig. 6 depicts the performance of the state-of-the-art schemes implemented in Sec. V.B versus time, for the scenario with  $N = 200$  nodes, with i.i.d. channels over frames. We evaluated the performance under both spatially-i.i.d. (solid lines) and spatially-correlated (dashed with markers) label scenarios. As also noted in the comments of Fig. 4, smaller

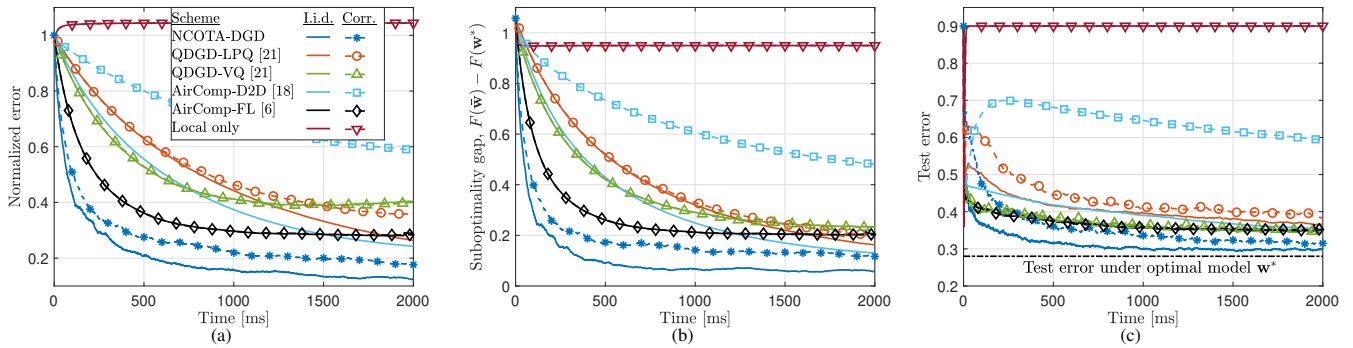


Fig. 6: Normalized error (a), suboptimality gap (b), test error (c) vs time, under both spatially-i.i.d. and correlated label scenarios, with i.i.d. channels over frames. Common legend shown in figure (a).

normalized error typically translates to smaller suboptimality gap and test error, and the performance generally degrades in the spatially-correlated scenario.

In both scenarios, we note that NCOTA-DGD achieves the best performance across time, followed by *AirComp-FL*. The worst performance is attained by *Local only*, since each node optimizes its local function and does not exploit inter-agent

communications. As noted in the comments of Sec. V.B, *AirComp-FL* benefits from its star-based topology: all communications happen to and from the parameter server, which maintains model synchronization across the network. However, this scheme also suffers from the same, due to the communication bottleneck experienced by the edge nodes, as discussed in Sec. V.B.